


Field-resilient superconductivity in atomic-layer crystalline materialsYoichi Higashi^{1,*}, Shunsuke Yoshizawa², Takashi Yanagisawa¹, Izumi Hase,¹
Yasunori Mawatari¹ and Takashi Uchihashi³¹National Institute of Advanced Industrial Science and Technology (AIST), Tsukuba, Ibaraki 305-8568, Japan²Center for Basic Research on Materials, National Institute for Materials Science (NIMS), 1-2-1 Sengen, Tsukuba, Ibaraki 305-0047, Japan³International Center for Materials Nanoarchitectonics (MANA),
National Institute for Materials Science (NIMS), 1-1 Namiki, Tsukuba, Ibaraki 305-0044, Japan (Received 27 July 2022; revised 18 May 2023; accepted 19 July 2023; published 9 August 2023)

A recent study [S. Yoshizawa *et al.*, *Nat. Commun.* **12**, 1462 (2021)] reported the occurrence of field-resilient superconductivity, that is, enhancement of the in-plane critical magnetic field H_{c2}^{\parallel} beyond the paramagnetic limiting field, in atomic-layer crystalline $(\sqrt{7} \times \sqrt{3})$ -In on a Si(111) substrate. The present article elucidates the origin of the observed field-resilient noncentrosymmetric superconductivity in this highly crystalline two-dimensional material. We develop the quasiclassical theory of superconductivity by incorporating the Fermi surface anisotropy together with an anisotropic spin splitting and texture specific to atomic-layer crystalline systems. In Si(111)- $(\sqrt{7} \times \sqrt{3})$ -In, a typical material with a large antisymmetric spin-orbit coupling (ASOC), we show an example where the combination of the ASOC and disorder effect suppresses the paramagnetic depairing and can lead to an enhancement of H_{c2}^{\parallel} compared to an isotropic system only when a magnetic field is applied in a particular direction due to an anisotropic spin texture. We also study the parity-mixing effect to demonstrate that the enhancement of H_{c2}^{\parallel} is limited in the moderately clean regime because of the fragile $s + p$ -wave pairing against nonmagnetic scattering in the case of the dominant odd-parity component of a pair wave function. Furthermore, from analysis of the transition line, we identify the field-resilience factor taking account of the scattering and suppression of paramagnetic effects and discuss the origin of the field-resilient superconductivity. Through fitting of the H_{c2}^{\parallel} data, the normal-state electron scattering is discussed with a prime focus on the role of atomic steps on a Si(111) surface.

DOI: [10.1103/PhysRevB.108.064504](https://doi.org/10.1103/PhysRevB.108.064504)**I. INTRODUCTION**

Highly crystalline atomic-layer materials are currently attracting significant research interest as a new phase of matter associated with two-dimensional (2D) systems [1–3]. The past decade has witnessed rapid progress in microfabrication technologies and atomic-layer materials research, as well as the development and integration of measurement techniques applicable at ultralow temperatures and ultrahigh vacuums. These advances have integrated superconductivity (SC) research and surface science, enabling the exploration of 2D SC by measuring the superconducting properties of highly crystalline atomic-layer materials.

Previous studies into 2D SC have been extensively conducted using ultrathin amorphous or highly disordered metal films [4–8]. In contrast to these systems, highly crystalline metal or alloy atomic-layer systems are fabricated on the reconstructions of semiconductor surfaces. The single-atomic-layer SC of Pb and In epitaxially grown on Si(111) surfaces has been observed by scanning tunneling spectroscopy [9]. Furthermore, a robust supercurrent was observed on a macroscopic scale by electron transport measurements on a reconstruction of the Si(111) surface with adsorbed In atoms [Si(111)- $(\sqrt{7} \times \sqrt{3})$ -In] [10]. Subsequently, the SC of

the single-atomic-layer alloy Si(111)- $(\sqrt{3} \times \sqrt{3})$ -Tl, Pb was confirmed by electron transport measurements [11]. Recently, the diamagnetic response of SC for Si(111)- $(\sqrt{7} \times \sqrt{3})$ -In was reported as well [12]. Herein, the $\sqrt{7} \times \sqrt{3}$ or $\sqrt{3} \times \sqrt{7}$ indicates the enlarged ratio of the surface superstructure unit cell to the bulk silicon crystal one.

Because the spatial inversion symmetry is intrinsically broken on a semiconductor substrate surface, heavy-element atomic layers on top of substrates accommodate spin-split energy bands owing to spin-orbit coupling (SOC) [13–16], which is referred to as antisymmetric SOC (ASOC) in the context of noncentrosymmetric SC [17]. Hence, the Fermi surface (FS) is allowed to split into two by lifting the spin degeneracy, and parity mixing of the pair wave function must occur, although its realization depends on the material parameters [18–20]. Indeed, spin-split metallic energy bands in the normal state have been observed by angle-resolved photoelectron spectroscopy (ARPES) for Si(111)- $(\sqrt{3} \times \sqrt{3})$ -Tl,Pb near the Fermi energy ε_F , with maximum energy splitting widths of 250 and 140 meV ($\sim 10^3 |\Delta|$) for the Σ_1 and Σ_2 bands, respectively [11,21], where $|\Delta|$ denotes the superconducting gap. Regarding Si(111)- $(\sqrt{7} \times \sqrt{3})$ -In, while the FS was observed by ARPES, spin-split energy bands were not because of the limited momentum resolution [22]. Recently, spin polarization on the butterfly-shaped FS was confirmed by spin-resolved ARPES, and the spin texture on the FS suggests a nonideal Rashba ASOC associated with the lower

*y.higashi@aist.go.jp

point group symmetry C_{1h} at the surface [23]. The maximum observed energy splitting at ε_F is 87 meV ($\sim 10^2 |\Delta|$), which is consistent with the results of density functional theory (DFT) calculations [23,24].

Meanwhile, the magnetic properties of atomic-layer SC have also been revealed. Suppression of paramagnetic depairing due to the Zeeman-type ASOC in Ising superconductors such as MoS_2 leads to significant enhancement of the in-plane critical field at zero temperature $H_{c2}^{\parallel}(T \approx 0)$, giving a maximum value in excess of 50 T [25]. For isotropic Rashba ASOC [26,27], H_{c2}^{\parallel} is limited to $\sqrt{2}H^P$ [28], where H^P is the conventional Pauli-limiting field. However, experimental results suggest H_{c2}^{\parallel} values well above H^P for $\text{Si}(111)\text{-In}$ ($\sqrt{7} \times \sqrt{3}$)-In [24].

Investigation of the influence of Pauli paramagnetism on the magnetic properties was pioneered by Maki, who scrutinized the role of spin-orbit scattering [29]. Several theoretical studies have elucidated the $T - H$ phase diagram for isotropic Rashba SC in the strong SOC regime to demonstrate the H_{c2}^{\parallel} enhancement upon increasing the density of Born scatterers [30–32] or introducing helical and stripe modulations [33–35]. For an arbitrary SOC strength, the enhancement of H_{c2}^{\parallel} under a helical modulation is shown in the dirty limit [36].

While most previous theories have been applied to isotropic systems [19,20,27,30–33,35–41], there are limited examples of their application to anisotropic systems such as bulk noncentrosymmetric crystals [42–44], oxide-heterostructure interfaces [45,46], and highly crystalline atomic-layer materials [25,47]. Highly crystalline atomic-layer materials possess anisotropic FSs that have ever been clearly observed with a spin texture structure. Because highly disordered alloys and amorphous thin films lack an anisotropic FS, this is an important feature for understanding the paramagnetic properties of atomic-layer SC. Furthermore, spin texture is not incorporated into the equation to determine H_{c2}^{\parallel} [29,48]. Therefore, the conventional isotropic description is unsatisfactory for explaining the H_{c2}^{\parallel} enhancement observed in highly crystalline atomic-layer superconductors.

In this study, by incorporating the anisotropic FS with spin texture obtained by DFT calculations and the parity-mixing effect, we develop the quasiclassical theory of SC by extending it to highly crystalline 2D superconductors. We apply the developed theory to the SC in $\text{Si}(111)\text{-}(\sqrt{7} \times \sqrt{3})\text{-In}$ to demonstrate the enhancement of $H_{c2}^{\parallel}(T \approx 0)$ to above $\sqrt{2}H^P$, that is, the occurrence of magnetic-field resilience. The enhancement of $H_{c2}^{\parallel}(T \approx 0)$ compared to an isotropic system results from the combination of the ASOC and disorder effect. It is not always present, but depends on the in-plane field direction due to an anisotropic spin texture. We also compare the numerical results with the available experimental data for $H_{c2}^{\parallel}(T \approx T_c)$ in $\text{Si}(111)\text{-}(\sqrt{7} \times \sqrt{3})\text{-In}$ for vicinal substrates and discuss the normal-state electron scattering off atomic steps.

The remainder of this paper is organized as follows. In Sec. II, we present the anisotropic FSs and spin texture on the butterfly-shaped FSs obtained by DFT calculations for $\text{Si}(111)\text{-}(\sqrt{7} \times \sqrt{3})\text{-In}$. Section III is devoted to the self-consistent equations based on the quasiclassical theory in the strong SOC regime, which is applicable to highly crystalline

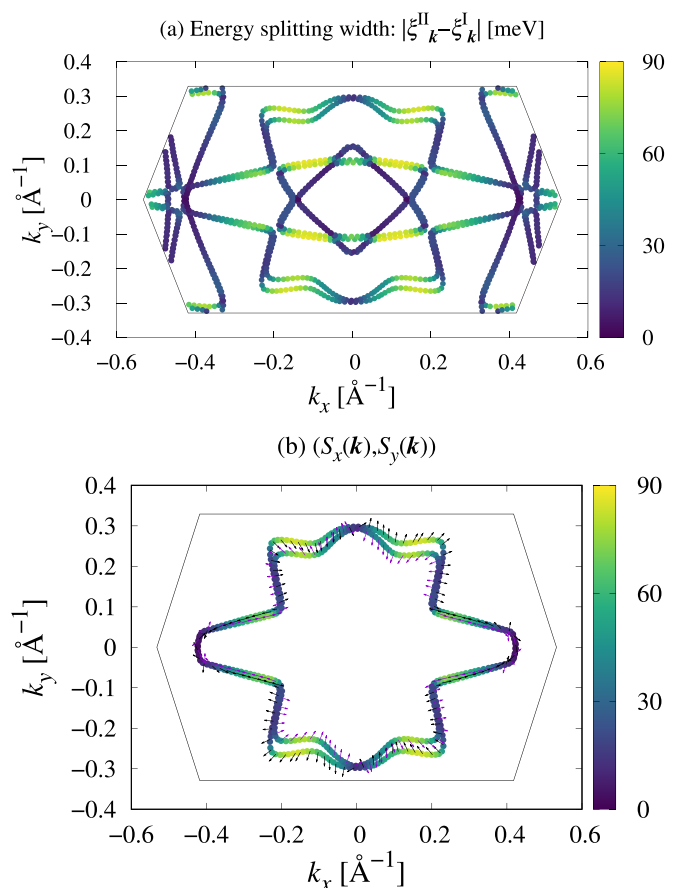


FIG. 1. (a) Anisotropic Fermi surface of $\text{Si}(111)\text{-}(\sqrt{7} \times \sqrt{3})\text{-In}$, where the color scale indicates the energy splitting width $|\xi_k^{\text{II}} - \xi_k^{\text{I}}|$. (b) Spin texture $(S_x(\mathbf{k}), S_y(\mathbf{k}))$ on the FSs with DOSs an order of magnitude larger than those for the other FSs. The solid line indicates the first Brillouin zone.

2D atomic-layer materials. In Sec. IV, we examine a parallel critical field and discuss the origin of the field resilience in $\text{Si}(111)\text{-}(\sqrt{7} \times \sqrt{3})\text{-In}$, and we also compare the numerical results for H_{c2}^{\parallel} with the experimental data to estimate the normal-state electron scattering rate. In Sec. V, the possible orbital effect and normal-state electron scattering are discussed with a focus on the role of atomic steps. Finally, a brief summary is provided in Sec. V.

II. ANISOTROPIC SPIN SPLITTING AND SPIN TEXTURE

Figure 1 depicts the energy splitting width and spin texture on the FS within the Brillouin zone for $\text{Si}(111)\text{-}(\sqrt{7} \times \sqrt{3})\text{-In}$, obtained by DFT calculations with SOC. These calculations were performed with the Quantum ESPRESSO suite of codes [49]. We employed the augmented plane wave method, and used the local density approximation for the exchange correlation. The crystal structure was modeled by a repeated slab, and the geometry optimization was performed without including the SOC. The resulting atomic coordinates show good agreement with diffraction measurements [50]. Further details on the computational conditions can be found in Refs. [24,50].

TABLE I. Densities of states (DOSs) at the Fermi level.

Band index	DOS ($\text{\AA}^{-2} \text{eV}^{-1}$)	Proportion (%)
396	5.46×10^{-3}	5.92
397	5.35×10^{-3}	5.80
398	9.45×10^{-3}	10.3
399	7.56×10^{-3}	8.20
400	2.33×10^{-2}	25.2
401	2.07×10^{-2}	22.4
402	6.92×10^{-3}	7.51
403	6.14×10^{-3}	6.66
404	3.61×10^{-3}	3.91
405	3.72×10^{-3}	4.04

The spin-split bands due to the SOC are denoted $\xi_k^{I,II}$, as described in more detail in Sec. III. As shown in Table I, the densities of states (DOSs) at ε_F for bands 400 and 401 are an order of magnitude larger than those for the other FSs. The proportions of the DOSs at ε_F to the total DOSs are 25.2% and 22.4% for bands 400 and 401, respectively. Thus, we focus on a single pair of the split FSs originating from bands 400 and 401 as shown in Fig. 1(b). This simplification is reasonable because the selected FSs dominate the superconducting properties, while the other FSs have an order of magnitude fewer states per unit energy contributing to the SC. The arrows on the FSs in Fig. 1(b) indicate the in-plane spin components ($S_x(\mathbf{k})$, $S_y(\mathbf{k})$).

Spin-split FSs in Rashba systems shift in an in-plane field, resulting in phase modulation of the pair wave function in space in the presence of a DOS difference between the split FSs (i.e., helical phase). The modulation wave number is evaluated via $q = 2\delta q_0$ with $q_0 = m^* \mu_B H / \hbar v_F$ [38] and $\delta = (N_I - N_{II}) / 2N_0 \approx 0.0589$ the DOS weighting factor for the FSs in Fig. 1(b). $N_{I,II}$ are the DOSs at ε_F for the spin-split bands and $N_0 = (N_I + N_{II}) / 2$. Correspondingly, the wavelength at 1 T is estimated as $\lambda = 2\pi / q \sim 867 \mu\text{m}$ by adopting $m^* = 1.14m_e$ and $\varepsilon_F = 6.60 \text{eV}$ in the free electron model, which gives rise to the material parameters $k_F = 1.41 \text{\AA}^{-1}$ and $v_F = 1.43 \times 10^6 \text{m/s}$ obtained by DFT calculations for Si(111)-($\sqrt{7} \times \sqrt{3}$)-In. The estimated λ is several hundred micrometers at several teslas, which is comparable to the sample size. Therefore, we neglect the helical modulation and focus instead on a uniform state in the long-wavelength limit to evaluate H_c^{\parallel} . This uniform state may survive against scatterers such as atomic defects in ($\sqrt{7} \times \sqrt{3}$)-In or the atomic steps inherent to a Si(111) substrate surface.

III. SELF-CONSISTENT EQUATIONS IN THE STRONG SPIN-ORBIT COUPLING LIMIT

We start with the normal-state Hamiltonian for 2D Rashba systems exposed to an in-plane field \mathbf{H} ,

$$\hat{\mathcal{H}}_n = \xi_k \hat{\sigma}_0 + [\lambda_k + \mu_B \mathbf{H}] \cdot \hat{\boldsymbol{\sigma}}, \quad (3.1)$$

where $\xi_k \equiv \varepsilon_k - \mu$ is the electron band energy measured from the chemical potential μ , λ_k is the vector characterizing the ASOC in energy units, μ_B is the Bohr magneton, and $\hat{\boldsymbol{\sigma}} =$

$(\hat{\sigma}_x, \hat{\sigma}_y, \hat{\sigma}_z)^\top$ is the vector of the Pauli spin matrices. The spin quantization axis is parallel to \mathbf{H} . The vector potential is disregarded because of the quenched orbital motion of electrons in the present configuration. Throughout the paper, $\hat{\cdot}$ denotes the 2×2 matrix in spin space. From now on, we set $\hbar = k_B = 1$.

By transforming Eq. (3.1) into the Hamiltonian in the band basis where $\hat{\mathcal{H}}_n$ in the absence of a magnetic field is diagonal, we obtain the eigenenergy for each band split owing to the ASOC:

$$E_k^{I,II} \approx \xi_k^{I,II} \pm \mu_B \bar{\lambda}_k \cdot \mathbf{H}, \quad (3.2)$$

where $\xi_k^{I,II} \equiv \xi_k \pm |\lambda_k|$ and $\bar{\lambda}_k \equiv \lambda_k / |\lambda_k|$. If we neglect the off-diagonal components describing the interband scattering induced by the in-plane field, the model reduces to the effective two-band model. By diagonalizing Eq. (3.1), we also obtain the excitation energy [Eq. (3.2)] up to the first order of $|\mu_B \mathbf{H}| / |\lambda_k|$. Herein, we assume $|\mu_B \mathbf{H}| / |\lambda_k| \ll 1$, which is met for the condition of atomic-layer superconductors with a sufficiently large ASOC, $|\lambda_k| \gg T_c$. The condition $|\mu_B \mathbf{H}| / |\lambda_k| \ll 1$ justifies the incorporation of the Zeeman field into the quasiclassical theory as a perturbation [41,51–54].

In the effective two-band model, we phenomenologically view the vector characterizing the ASOC to be defined for each band: $\lambda_k \rightarrow \lambda_k^l$ with $l = I$ or II denoting the band index. The ASOC is characterized through $\lambda_k^l = \sqrt{\langle |\lambda_k^l|^2 \rangle_k} \mathbf{g}_k^l$ by the antisymmetric orbital vector

$$\mathbf{g}_k^l = \frac{|\Delta \xi_k^l|}{\sqrt{\langle |\Delta \xi_k^l|^2 \rangle_0}} \frac{\mathbf{S}_k^l}{|\mathbf{S}_k^l|}, \quad (3.3)$$

which is set to be normalized as $\langle (\mathbf{g}_k^l)^2 \rangle_0 = 1$ in accordance with an isotropic Rashba system. In Eq. (3.3), $|\Delta \xi_k^l| / \sqrt{\langle |\Delta \xi_k^l|^2 \rangle_0}$ represents the anisotropy of the spin-split energy relative to the typical energy scale of the ASOC. Here, $\langle \dots \rangle_0$ denotes an average over the FS in the absence of the ASOC and \mathbf{H} : $\langle \dots \rangle_0 \equiv \int dS_{F0}^l(\mathbf{k}) |v_{F0}^l(\mathbf{k})|^{-1} \dots / \int dS_{F0}^l(\mathbf{k}) |v_{F0}^l(\mathbf{k})|^{-1}$ with $dS_{F0}^l(\mathbf{k})$ and $v_{F0}^l(\mathbf{k})$ the infinitesimal line element of the 2D FS and the Fermi velocity in the absence of the ASOC and \mathbf{H} , respectively. $|\Delta \xi_k^l| \equiv |\xi_k^I - \xi_k^{II}|$ is the energy splitting width. The maximum spin-split energy is $|\Delta \xi^{400}| \approx 84 \text{meV}$ and $|\Delta \xi^{401}| \approx 80 \text{meV}$ for the bands 400 and 401, respectively. By adopting experimental value of the transition temperature $T_c^{\text{vicinal}}(0) \approx 3.05 \text{K}$ at zero field for ($\sqrt{7} \times \sqrt{3}$)-In on a vicinal Si(111) surface, the maximum value of ASOC is estimated as $|\Delta \xi^{400}| / T_c^{\text{vicinal}}(0) \approx 320$ and $|\Delta \xi^{401}| / T_c^{\text{vicinal}}(0) \approx 302$ for the bands 400 and 401, respectively. The momentum-dependent spin polarization vector is obtained as in Fig. 1(b) through $\mathbf{S}_k^l = (1/2) \langle \Psi_k^l | \hat{\boldsymbol{\sigma}} | \Psi_k^l \rangle$ from the DFT calculations, where $|\Psi_k^l\rangle$ is the eigenstate of Eq. (3.1) at $\mathbf{H} = \mathbf{0}$.

The parity-mixed superconducting order parameters are determined via the self-consistent equations (B30) and (B31), which are suitable for equivalent FSs (i.e., infinitesimally split FSs) in the weak-ASOC limit as proposed in Ref. [40]. However, in the strong-ASOC limit, the significantly split FSs are no longer equivalent. Consequently, the average on the FS should be taken for each FS. Thus, Eqs. (B30) and (B31)

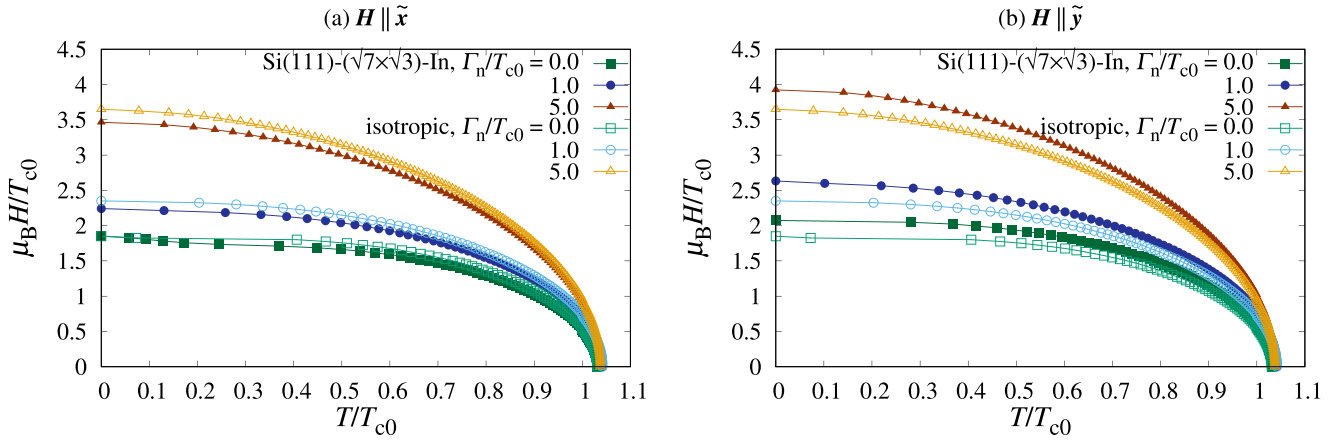


FIG. 2. Temperature dependence of an in-plane critical magnetic field oriented parallel to the (a) x and (b) y axes for s -wave pairing upon varying the normal-state scattering rate Γ_n . The filled and open symbols represent the data for the FS of Si(111)- $(\sqrt{7} \times \sqrt{3})$ -In and an isotropic system, respectively. The difference in the DOSs between the two split FSs is set to $\delta = 0$.

are recast as

$$\psi_s = \frac{\pi T}{2} \sum_{n=-[n_c(T)]-1}^{[n_c(T)]} [\lambda_s \{(1 + \delta)\langle f_I \rangle_I + (1 - \delta)\langle f_{II} \rangle_{II}\} + \lambda_m \{(1 + \delta)\langle |g_k^I| f_I \rangle_I - (1 - \delta)\langle |g_k^II| f_{II} \rangle_{II}\}], \quad (3.4)$$

$$d_t = \frac{\pi T}{2} \sum_{n=-[n_c(T)]-1}^{[n_c(T)]} [\lambda_m \{(1 + \delta)\langle f_I \rangle_I + (1 - \delta)\langle f_{II} \rangle_{II}\} + \lambda_t \{(1 + \delta)\langle |g_k^I| f_I \rangle_I - (1 - \delta)\langle |g_k^II| f_{II} \rangle_{II}\}], \quad (3.5)$$

where $[n_c(T)]$ indicates the integer part of $n_c(T) = (\omega_c/\pi T - 1)/2$ with the cutoff frequency set to $\omega_c = 7\pi T_{c0}$ for the numerical calculations throughout the paper. Here, $T_{c0} \equiv (2\omega_c e^\gamma/\pi) e^{-1/\lambda}$, where $\gamma = 0.577\dots$ is the Euler constant and is determined via $\frac{1}{\lambda} \equiv \sum_{n=0}^{[n_c(T_{c0})]} 1/(n + 1/2)$. The quasiclassical Green's functions g_l and f_l ($l = I, II$) are given in Appendix A. In the limit of $T \rightarrow T_c$, the coupling constants for the spin singlet and triplet attraction force channels are determined from the linearized gap equation at $\mathbf{H} = \mathbf{0}$ in the clean limit through

$$\lambda_s = \frac{2\lambda\nu - \lambda_m \{(1 + \delta)\nu\langle |g_k^I| \rangle_I - (1 - \delta)\nu\langle |g_k^II| \rangle_{II} + (1 + \delta)\langle |g_k^I|^2 \rangle_I + (1 - \delta)\langle |g_k^II|^2 \rangle_{II}\}}{2\nu + (1 + \delta)\langle |g_k^I| \rangle_I - (1 - \delta)\langle |g_k^II| \rangle_{II}}, \quad (3.6)$$

$$\lambda_t = \frac{2\lambda - \lambda_m \{2\nu + (1 + \delta)\langle |g_k^I| \rangle_I - (1 - \delta)\langle |g_k^II| \rangle_{II}\}}{(1 + \delta)\nu\langle |g_k^I| \rangle_I - (1 - \delta)\nu\langle |g_k^II| \rangle_{II} + (1 + \delta)\langle |g_k^I|^2 \rangle_I + (1 - \delta)\langle |g_k^II|^2 \rangle_{II}}, \quad (3.7)$$

respectively, where λ_m is the coupling constant for the mixing channel, $\nu = \psi_s/d_t|_{T \rightarrow T_{c0}}$ is the parity-mixing ratio, and

$$\frac{1}{\lambda} \approx \ln\left(\frac{T}{T_{c0}}\right) + \sum_{n=0}^{[n_c(T)]} \frac{2}{2n + 1}. \quad (3.8)$$

IV. NUMERICAL RESULTS

A. Transition line

We numerically solve Eqs. (B30) and (B31) [or Eqs. (3.4) and (3.5)] for an isotropic [or Si(111)- $(\sqrt{7} \times \sqrt{3})$ -In] FS in an iterative manner to achieve self-consistency, $\Delta Q < 1 \times 10^{-6}$. Here, $\Delta Q \equiv \max_{i\omega_n} [|Q_{\text{new}}(i\omega_n) - Q_{\text{old}}(i\omega_n)|]$ with $Q(i\omega_n)$ being ψ_s , d_t , $\sigma_g(i\omega_n)$, or $\sigma_f(i\omega_n)$. We use the bisection method for $\text{Re}[\psi_s(d_t)(T, \mathbf{H})] - \varepsilon = 0$ to obtain the numerical solutions of $H_{c2}^{\parallel}(T)$ for $0.05T_{c0} \leq T \leq 1.2T_{c0}$. The numerical solution at low temperature ($T < 0.05T_{c0}$) is regarded as $H_{c2}^{\parallel}(0)$. The constant energy shift used in the bisection

method is always set to $\varepsilon/T_{c0} = 1 \times 10^{-4}$. The DOS difference between the split FSs is set to $\delta = 0$ in accordance with a uniform state. In the presence of the DOS difference, the contribution of the outer FS I originating from the band 400 with a larger DOS at ε_F becomes more prominent, and therefore the spin structure on the outer FS I is more influential for H_{c2}^{\parallel} .

Figures 2(a) and 2(b) show the temperature dependence of an in-plane critical magnetic field $H_{c2}^{\parallel}(T)$ in the case of an s -wave pairing for $\mathbf{H} \parallel \tilde{\mathbf{x}}$ and $\mathbf{H} \parallel \tilde{\mathbf{y}}$, respectively. Here, $\tilde{\mathbf{x}}$ ($\tilde{\mathbf{y}}$) denotes the unit vector in the direction of the x (y) axis, taken to be parallel to the k_x (k_y) direction in Fig. 1. For both the Si(111)- $(\sqrt{7} \times \sqrt{3})$ -In and isotropic FSs, H_{c2}^{\parallel} is enhanced with increasing Γ_n irrespective of the field direction, in accordance with the results reported by Dimitrova and Feigel'man for an s -wave pairing on an isotropic FS [31]. No change in the superconducting transition temperature at zero field $T_c(0)$ against nonmagnetic scattering reflects

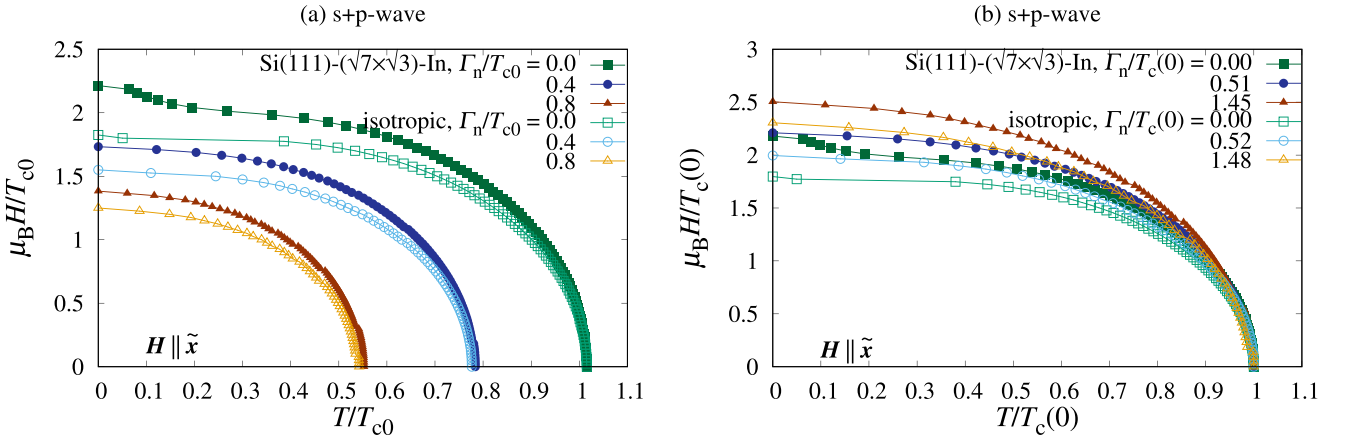


FIG. 3. Temperature dependence of an in-plane critical magnetic field oriented parallel to the x axis for the $s + p$ -wave pairing upon varying the normal-state scattering rate Γ_n . The filled and open symbols represent the data for the FS of Si(111)-($\sqrt{7} \times \sqrt{3}$)-In and an isotropic system, respectively. The difference in the DOSs between the two split FSs is set to $\delta = 0$. The parity-mixing ratio and the coupling constant for the mixing channel are $\nu = 0.5$ and $\lambda_m = 0.1$, respectively. The temperature and magnetic field are normalized by (a) T_{c0} and (b) $T_c(0)$, respectively.

Anderson's first theorem [55,56]. For 2D superconductors such as ultrathin amorphous films, as the film thickness is reduced, the disorder and quantum fluctuations of the superconducting phase increase, forming localized unpaired electrons, which lead to the suppression of T_c [4–6,57]. Here, for the sake of simplicity, we disregarded such effects because disorder is weak in a highly crystalline atomic layer judging from the small value of the normal-state sheet resistance, and a sharp transition to SC was observed by electron transport measurements [24]. As shown in Fig. 2(a), for $\mathbf{H} \parallel \tilde{x}$, $H_{c2}^{\parallel}(T)$ was larger for the isotropic FS than for the Si(111)-($\sqrt{7} \times \sqrt{3}$)-In FS. By contrast, as shown in Fig. 2(b), for $\mathbf{H} \parallel \tilde{y}$, $H_{c2}^{\parallel}(T)$ was larger for the Si(111)-($\sqrt{7} \times \sqrt{3}$)-In FS than for the isotropic FS over the entire temperature range. Thus, in the case of the anisotropic FS, H_{c2}^{\parallel} is not always enhanced. The enhancement depends on the relation between the field direction and the spin structure on the FS.

Figures 3(a) and 3(b) present plots of $H_{c2}^{\parallel}(T)$ normalized by T_{c0} and $T_c(0)$, respectively, in the case of $s + p$ -wave pairing for $\mathbf{H} \parallel \tilde{x}$. Note that $H_{c2}^{\parallel}(T)$ for ψ_s and d_t show almost the same profile, but the amplitudes of ψ_s and d_t vary depending on the parity-mixing parameters ν and λ_m . Here, they are set to $\nu = 0.5$ (i.e., dominant p -wave component d_t) and $\lambda_m = 0.1$, respectively. The variation of the transition line upon changing ν and λ_m is discussed in Appendix C. As shown in Fig. 3(a), nonmagnetic scattering is detrimental to T_c because of the dominance of d_t over ψ_s . More specifically, by examining the linearized gap equation in the case of parity mixing, we notice that the scale factors of the following quantities are different as long as ν is finite:

$$1 + \frac{\sigma_g}{\omega_n} = 1 + \frac{\Gamma_n}{|\omega_n|} \equiv \eta(\omega_n), \quad (4.1)$$

$$1 + \frac{\sigma_f}{\psi_s} = \eta(\omega_n) \left(1 + \frac{\delta}{\nu} \right) - \frac{\delta}{\nu}. \quad (4.2)$$

Therefore, the scale factors of Eqs. (4.1) and (4.2) in the anomalous Green's function do not cancel out, and thus the nonmagnetic scattering affects T_c . Figure 3(b) shows

that the enhancement of $\mu_B H_{c2}^{\parallel}/T_c(0)$ with increasing Γ_n remains, but it is rather weak in the case of the dominant p -wave pairing compared with the pure s -wave pairing [31] [see Fig. 2(a)].

The clean-limit data for the isotropic FS (open squares) in Fig. 3(b), $\mu_B H_{c2}^{\parallel}(T \approx 0)/T_c(0)$, show the Pauli-limiting field for an isotropic Rashba system, which is estimated via $\sqrt{2}H^P \approx 1.77T_c(0)/\mu_B$ with $H^P = \sqrt{2}\psi_s/g\mu_B$ as the conventional Pauli-limiting field. We use the weak-coupling Bardeen-Cooper-Schrieffer (BCS) ratio and the electronic g factor, $g = 2$. Thus, $H_{c2}^{\parallel}(T \approx 0)$ clearly exceeds $\sqrt{2}H^P$. It turns out that the $H_{c2}^{\parallel}(T \approx 0)$ enhancement appears also in the dominant p -wave case. The enhancement of $H_{c2}^{\parallel}(T \approx 0)$ is a result from both the anisotropic spin texture and disorder effect.

In the case of $\mathbf{H} \parallel \tilde{y}$ (Fig. 4), $\mu_B H_{c2}^{\parallel}/T_c(0)$ is also enhanced with increasing Γ_n , but in the case of the anisotropic FS this enhancement is suppressed, in contrast to the case of $\mathbf{H} \parallel \tilde{x}$. The H_{c2}^{\parallel} enhancement is dependent on the in-plane field direction, demonstrating that the anisotropic spin texture does not always increase H_{c2}^{\parallel} .

A slight upturn of H_{c2}^{\parallel} at low temperatures is observed in Figs. 2–4 for Si(111)-($\sqrt{7} \times \sqrt{3}$)-In in the clean limit. Because this behavior is absent in the isotropic Rashba system, it is ascribed to the anisotropic spin splitting and spin texture as illustrated in Fig. 1. With increasing Γ_n , the anisotropic feature is considered to be washed out, resulting in no upturn of H_{c2}^{\parallel} as observed in the data for $\Gamma_n \neq 0$ in Figs. 2–4. An upturn of H_{c2}^{\parallel} in the absence of helical modulation was also reported in Ref. [46], although it was attributed to the orbital degrees of freedom together with the Rashba SOC.

B. Magnetic-field resilience

The first equation for determining $H_{c2}(T)$ in superconductors with Pauli paramagnetism was derived by incorporating the SOC only through the spin-orbit scattering time [29,48].

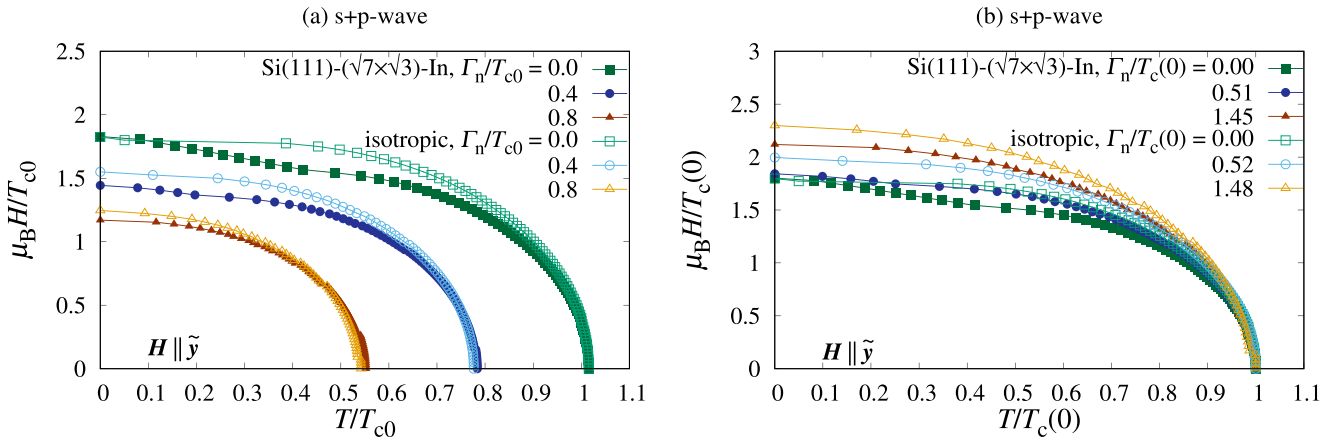


FIG. 4. Temperature dependence of an in-plane critical magnetic field oriented parallel to the y axis for the $s + p$ -wave pairing upon varying the normal-state scattering rate Γ_n . The filled and open symbols represent the data for the FS of Si(111)- $(\sqrt{7} \times \sqrt{3})$ -In and an isotropic system, respectively. The difference in the DOSs between the two split FSs is set to $\delta = 0$. The parity-mixing ratio and the coupling constant for the mixing channel are $\nu = 0.5$ and $\lambda_m = 0.1$, respectively. The temperature and magnetic field are normalized by (a) T_{c0} and (b) $T_c(0)$, respectively.

Later, in the clean limit, an equation for $H_{c2}(T)$ with the textured spin structure being explicitly incorporated was obtained [20,37,58], thereby allowing the suppression of the paramagnetic depairing by the SOC to be discussed. The $H_{c2}^{\parallel}(T)$ line was computed for the 2D Rashba model taking

account of the contribution that is not incorporated into the impurity self-energy [31]. Below, we present the analytic expression for $H_{c2}^{\parallel}(T \approx T_c(0))$ in the case of parity mixing, taking account of both the impurity scattering and suppression of paramagnetic depairing:

$$\frac{T_c(0) - T_c}{T_c(0)} = \frac{\zeta(3, 1/2 + \gamma_n)}{4\pi^2} \frac{\mu_B^2 \langle (\tilde{\mathbf{g}}_{\mathbf{k}} \cdot \mathbf{H})^2 \rangle_{\mathbf{k}}}{T_c^2(0)} + \frac{\lambda_s - (1 + \delta)[\lambda_s(1 + \langle |\mathbf{g}_{\mathbf{k}}| \rangle / \nu) + \lambda_m(\langle |\mathbf{g}_{\mathbf{k}}| \rangle + 1/\nu)]}{\lambda_s(1 + \delta)(\lambda_s + \lambda_m)(1 + 1/\nu)}, \quad (4.3)$$

where $\gamma_n \equiv \Gamma_n/2\pi T_c(0)$ and $\zeta(z, a) = \sum_{n=0}^{\infty} 1/(a+n)^z$ ($z \in \mathbb{C}$, a : constant) is the Hurwitz zeta function. Note that Eq. (4.3) is derived by assuming that the FS is infinitesimally split and $|\tilde{\mathbf{g}}_{\mathbf{k}} \cdot \mu_B \mathbf{H} / \pi T_c| \ll 1$. In Eq. (4.3), $T_c(0)$ should be read as the zero-field transition temperature without the parity mixing and the DOS difference. For generic cases characterized by the antisymmetric orbital vector $\mathbf{g}_{\mathbf{k}}$, the effective field is $H_{\text{eff}} \equiv H_{\mu}/R_{\mu}$ with

$$R_{\mu} \equiv \left[\frac{\zeta(3, 1/2 + \gamma_n)}{7\zeta(3)} \langle g_{\mu}^2(\tilde{\mathbf{k}}) \rangle_{\mathbf{k}} \right]^{-1/2} \quad (4.4)$$

for $\mathbf{H} \parallel \tilde{\boldsymbol{\mu}}$. Consequently, the Pauli-limiting field ($\parallel \tilde{\boldsymbol{\mu}}$) is determined via $H_{\text{eff}} = H^P$ as

$$H_{\mu}^P = R_{\mu} H^P. \quad (4.5)$$

The physical meaning of R_{μ} is interpreted as the *magnetic-field resilience* of SC for H_{μ} . The H_{c2}^{\parallel} enhancement from $\sqrt{2}H^P$ is roughly judged from the condition that $\langle g_{\mu}^2(\tilde{\mathbf{k}}) \rangle_{\mathbf{k}} < 1/2$. The dependence of R_{μ} on Γ_n is plotted in Fig. 5. When evaluating Eq. (4.4), we phenomenologically replace the average on the infinitesimally split FS $\langle \dots \rangle_{\mathbf{k}}$ with that on the significantly split FSs I and II $\langle \dots \rangle_{\text{I,II}}$ to apply R_{μ} to the FS of Si(111)- $(\sqrt{7} \times \sqrt{3})$ -In (In/Si). R_{μ} increases monotonically with respect to Γ_n , in accordance with the H_{c2}^{\parallel} enhancement with increasing Γ_n . For $\mathbf{H} \parallel \tilde{\mathbf{x}}$, the R_x values for both of the In/Si FSs I and II are larger than R_{μ} for the isotropic Rashba

system. However, in the case of $\mathbf{H} \parallel \tilde{\mathbf{y}}$, the magnitude of R_y for In/Si relative to that for the isotropic Rashba system depends on the details of the FS and the spin texture, as reflected in $\langle g_y^2(\tilde{\mathbf{k}}) \rangle_{\text{I}} = 0.455 < 1/2$ and $\langle g_y^2(\tilde{\mathbf{k}}) \rangle_{\text{II}} = 0.646 > 1/2$.

In the absence of parity mixing ($\lambda_m = 0$ and $\nu \rightarrow \infty$) and the DOS difference between the split FSs ($\delta = 0$), Eq. (4.3) for an isotropic 2D Rashba superconductor [$\tilde{\mathbf{g}}_{\mathbf{k}} = (-\sin \phi_{\mathbf{k}}, \cos \phi_{\mathbf{k}}, 0)$] in the clean limit ($\gamma_n = 0$) reduces to the

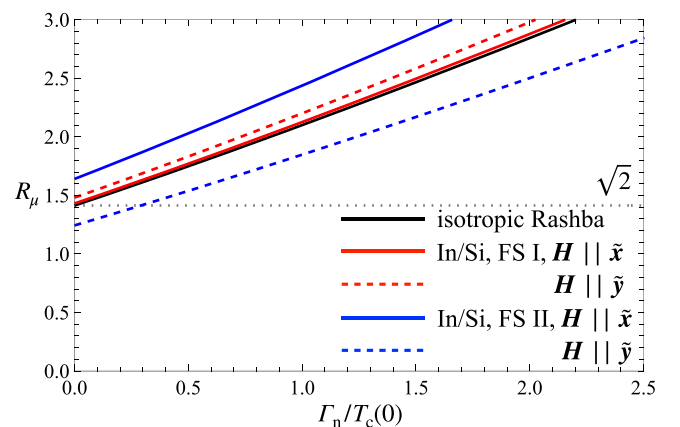


FIG. 5. Dependence of the field-resilience factor R_{μ} on Γ_n for the isotropic Rashba system and Si(111)- $(\sqrt{7} \times \sqrt{3})$ -In (In/Si).

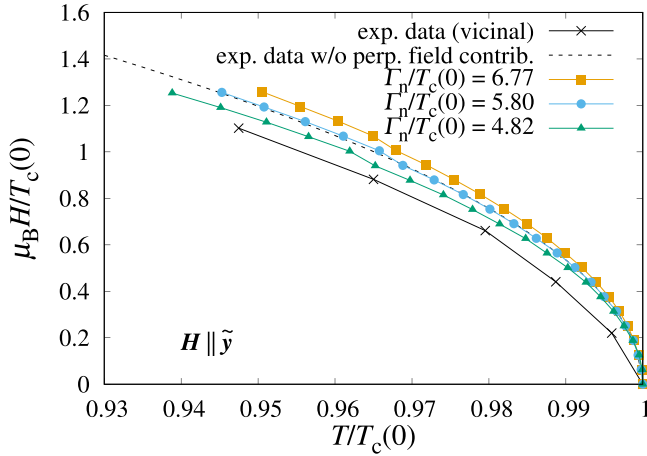


FIG. 6. Comparison of the theoretically evaluated in-plane critical magnetic field for the s -wave pairing with the experimental data for the $(\sqrt{7} \times \sqrt{3})$ -In sample on a vicinal Si(111) surface. The magnetic field is parallel to the y axis. The difference in the DOSs between the two split FSs is $\delta = 0.0589$.

result reported by Barzykin and Gor'kov [37]:

$$\frac{T_c(0) - T_c}{T_c(0)} = \frac{7\zeta(3)}{4\pi^2} \frac{\mu_B^2 (H/\sqrt{2})^2}{T_c^2(0)}. \quad (4.6)$$

Here, $\sqrt{(\mathbf{g}_k \cdot \mathbf{H})^2}_{\mathbf{k}} = H/\sqrt{2}$ can be viewed as an effective field for the isotropic Rashba SC. Thus, the enhancement of the Pauli-limiting field is limited to $\sqrt{2}H^P$.

C. Comparison with experimental $H_{c2}^{\parallel}(T)$ data

In Fig. 6, the experimental $H_{c2}^{\parallel}(T)$ data for Si(111)- $(\sqrt{7} \times \sqrt{3})$ -In are compared with the numerical data for an s -wave pairing. The field direction is set to $\mathbf{H} \parallel \tilde{y}$ in accordance with the experimental setup. For the pair of split FSs with DOSs an order of magnitude larger than the others [see Fig. 1(b)], the DOS difference is evaluated as $\delta = 0.0589$ by DFT calculations. By subtracting a perpendicular field component [$H_{c2}^{\perp}(T) \propto T_c(0) - T$] from the experimental $H_{c2}^{\parallel}(T \approx T_c(0))$ data, we may compare the numerical calculation results with the contribution from the in-plane field responsible for paramagnetic depairing in the experimental data. The experimental data of the parallel field contribution (dashed line in Fig. 6) are in good agreement with the numerical data for $\Gamma_n/T_c(0) \approx 5.8$ in the case of an s -wave pairing. Assuming the parabolic dependence $T/T_c(0) = 1 - c[\mu_B H/T_c(0)]^2$, we identify the quadratic coefficients c_{exp} and c_{num} for the experimental and numerical $H_{c2}^{\parallel}(T)$ data, respectively. Regarding c_{num} for each Γ_n , we obtain $c_{\text{num}}(\Gamma_n)$ by polynomial fitting. By solving $c_{\text{num}}(\Gamma_n) = c_{\text{exp}}$, we obtain the more precise value of $\Gamma_n/T_c(0) \approx 5.9$, which is consistent with the previous study [31]. From the low-field data of $H_{c2}^{\parallel}(T)$, one can quantitatively estimate the normal-state scattering rate.

On the basis of Eq. (4.3), in the absence of parity mixing ($\nu \rightarrow \infty$ and $\lambda_m = 0$) and the DOS difference ($\delta = 0$), the quadratic coefficient for an isotropic Rashba system is

obtained as

$$c(\Gamma_n) = \frac{\zeta(3, 1/2 + \gamma_n)}{8\pi^2}. \quad (4.7)$$

By solving $c(\Gamma_n) = c_{\text{exp}}$, we obtain $\Gamma_n/T_c(0) \approx 1.5$. Thus, Eq. (4.3) somewhat underestimates Γ_n compared with the numerically estimated value. This is because Eq. (4.3) is derived by assuming infinitesimally split FSs, and thus strictly speaking it is not directly applicable to a system in the large-ASOC regime.

V. DISCUSSION

In the evaluation of H_{c2}^{\parallel} with the developed quasiclassical theory in the strong-ASOC limit, we assume some additional approximations that ignore the following phenomena: (a) phase modulation in the helical state, (b) localized unpaired electrons due to disorders and quantum fluctuations in 2D systems, (c) scattering off atomic steps and interatomic-terrace orbital motion. In the following, we first discuss (c) and lastly give a physical picture of how the spin texture on the FS and the disorder support the field-resilient superconductivity.

A. Interatomic-terrace orbital effect

The SC of Si(111)- $(\sqrt{7} \times \sqrt{3})$ -In can be affected by possible orbital effects in an in-plane field in the case of high atomic step density. For a vicinal substrate, the atomic step density may be as high as approximately 20/500 nm [24]. Thus, the total atomic step height may reach several micrometers ($\sim 100\xi$) over the sample size by assuming the same height of approximately 0.3 nm [59] for all of the atomic steps. For a vicinal substrate, we herein estimate the effective coherence length as $\xi \sim 40$ nm via $1/\xi = 1/\xi_{\text{BCS}} + 1/v_F\tau_{\text{el}}$ using the following adopted parameters: $\Delta = 0.39$ meV [60], $v_F = 1.43 \times 10^6$ m/s (see Sec. II), and $\tau_{\text{el}} \sim 30$ fs [24], with $\xi_{\text{BCS}} = v_F/\pi\Delta$ denoting the BCS coherence length and τ_{el} representing the elastic scattering time. Under these circumstances, the orbital motion of electrons may be allowed owing to the sufficient thickness of the atomic terraces. An indium atomic bilayer itself is considered not to be responsible for the orbital motion under an in-plane field. How an in-plane critical field depends on *interatomic-terrace orbital effects* currently remains unresolved.

In the theoretical model, we assume a Si(111) substrate with a low atomic step density, that is, an atomically flat plane on a terrace that is as large as ξ . We also assume that the field direction is parallel to the long dimension of the atomic terraces to avoid possible interatomic terrace orbital effects, although in reality there are several thousand atomic steps over the sample size even when the field is parallel to the long dimension of the atomic terraces because of the inevitable error in the cutout angle of a Si(111) substrate. In this study, for simplicity, we neglect the interatomic-terrace orbital effect in the theoretical model to show the enhancement of H_{c2}^{\parallel} , suggesting that, from a theoretical perspective, the electron scattering off atomic steps inherent to a Si(111) substrate surface is not primarily responsible for the H_{c2}^{\parallel} enhancement.

The scattering from disorder within the flat atomic terrace plane may be more important for H_{c2}^{\parallel} enhancement.

B. Scattering rate via fitting analysis and electron transport

For a flat Si(111) substrate, there are three crystallographic orientations in the $\sqrt{7} \times \sqrt{3}$ structures [24], while for a vicinal substrate cut from bulk Si(111) with a misangle from a certain direction, the crystallographic orientation of the $(\sqrt{7} \times \sqrt{3})$ -In is aligned in the same direction. The atomic step density is higher on the vicinal surface than on the flat surface, meaning that the density of electron scatterers is also higher. Indeed, the rate of elastic electron scattering events in the normal state, Γ_n , for $(\sqrt{7} \times \sqrt{3})$ -In samples on the vicinal substrate exhibits larger values. From the inelastic scattering time evaluated by electron transport measurements for three different samples [24], Γ_n falls in the range of $\Gamma_n/T_c(0) = 17$ –27 for the flat substrate. By contrast, for the vicinal substrate, $\Gamma_n/T_c(0) = 32$ –45. The values of Γ_n estimated via the normal-state sheet resistance are an order of magnitude larger than the value of $\Gamma_n/T_c(0) \approx 5.9$ obtained from the fitting analysis of the low-field H_{c2}^{\parallel} data for the $(\sqrt{7} \times \sqrt{3})$ -In sample on a vicinal Si(111) surface.

Electron transport measurements over the sample size include the contribution from the scattering off atomic steps on the Si(111) surface. However, the theoretical model does not explicitly incorporate atomic steps as a scattering source, and instead disordered regions are assumed to be weak scatterers and randomly distributed in the system. Thus, the value of Γ_n evaluated via the electron transport measurements may be overestimated as an indicator of the effects of disorder on the SC of atomic-layer crystalline $(\sqrt{7} \times \sqrt{3})$ -In. Within atomically flat terraces, highly crystalline $(\sqrt{7} \times \sqrt{3})$ -In may be effectively much cleaner than observed from the electron transport. Indeed, H_{c2}^{\parallel} in the case of the vicinal substrate is not substantially different from the value for a flat substrate, although the H_{c2}^{\parallel} enhancement is expected for the vicinal substrate because of the increased number of scattering events due to the higher atomic step density. This fact possibly supports the theoretical consideration regarding the effectively small Γ_n within atomic terraces. In the present analysis, we adopted Born-type scatterers to model weak disorder within atomic terraces. At the atomic steps, we speculate that the electron scattering is not simple forward scattering in the Born limit. Instead, scattering with an arbitrary scattering phase including backward scattering in the unitary limit may occur. The influence of such a scattering process on H_{c2}^{\parallel} remains unknown.

C. Physical picture of field-resilient superconductivity

We discuss the physics of the field-resilient SC. For simplicity, we consider an *s*-wave pairing on each split isotropic FS without the DOS difference. In the limit of large SOC, the split isotropic FSs are regarded as equivalent, and therefore the average on each split FS can be merged. The impurity self-energies are evaluated via the Green's functions at the zero field in the clean limit as $\sigma_g \approx \Gamma_n$ ($\omega_n > 0$) and $\sigma_f \approx (\Gamma_n/\omega_n)\psi_s$. Keeping σ_f in the numerator of the anomalous

Green's function $f_{I,II}$, the linearized gap equation reads

$$\frac{1}{\lambda_s} = 2\pi T_c \sum_{\omega_n > 0} \left\langle \frac{1}{\omega_n} \frac{1}{1 + [\bar{\mathbf{g}}_k \cdot \mu_B \mathbf{H}/(\omega_n + \Gamma_n)]^2} \right\rangle_{\bar{\mathbf{k}}}. \quad (5.1)$$

We observe the complete suppression of the paramagnetic depairing for $\bar{\mathbf{g}}_k \cdot \mu_B \mathbf{H} = 0$, but even when $\bar{\mathbf{g}}_k \cdot \mu_B \mathbf{H} \neq 0$, with increasing Γ_n the influence of the magnetic field effectively gets smaller to suppress the paramagnetic depairing. As described in Refs. [24,45,61], this can be interpreted as follows. Due to intraband nonmagnetic impurity scattering, the spin quantization axis of electrons traveling in the \mathbf{k} direction is not fixed in the $\bar{\mathbf{g}}_k$ direction, but it is forced to rotate in the $\bar{\mathbf{g}}_k$ direction to partially escape from the paramagnetic depairing. In the Rashba SC with the large ASOC under an in-plane field, the intraband states $(\mathbf{k}, \hat{\sigma} \cdot \bar{\mathbf{g}}_k)$ and $(-\mathbf{k}, \hat{\sigma} \cdot \bar{\mathbf{g}}_{-k})$ pair up with a finite energy difference to form the zero center-of-mass momentum superconducting state. In the energy domain, due to the impurity scattering the energy bands near the Fermi energy have an energy broadening, allowing the states with smaller energy differences to be paired up with the zero center-of-mass momentum to higher magnetic fields. In this way, the Rashba SC acquires the field resilience.

VI. SUMMARY

To study the SC in highly crystalline atomic-layer materials, we formulated the quasiclassical theory of SC in the large-ASOC regime with the incorporation of parity mixing, FS anisotropy, and spin texture. We applied the developed theory to the atomic-layer crystalline material Si(111)- $(\sqrt{7} \times \sqrt{3})$ -In to calculate the in-plane critical magnetic field H_{c2}^{\parallel} upon varying the normal-state scattering rate Γ_n . For Si(111)- $(\sqrt{7} \times \sqrt{3})$ -In, we proceeded with the typical scenario of possible H_{c2}^{\parallel} enhancement. In accordance with the previous study [31], when Γ_n is increased, H_{c2}^{\parallel} was enhanced in combination with the ASOC. We found that this trend holds also in the case of parity mixing. Furthermore, we demonstrated that the H_{c2}^{\parallel} enhancement is dependent on the field direction, meaning that the anisotropic FS and spin texture do not always enhance H_{c2}^{\parallel} . To quantify the H_{c2}^{\parallel} enhancement relative to the Pauli-limiting field for an isotropic Rashba SC, we proposed the *magnetic-field resilience* of SC, which incorporates impurity scattering and details of the FS and spin texture. Next, we extracted the value of Γ_n by numerically and analytically fitting the experimental H_{c2}^{\parallel} data for a $(\sqrt{7} \times \sqrt{3})$ -In sample on a vicinal Si(111) surface. Finally, the possible interatomic-terrace orbital effect and normal-state electron scattering were discussed focusing on the role of atomic steps.

ACKNOWLEDGMENTS

We thank S. Ichinokura for discussions in the early stage of the research. The numerical calculations were performed on XC40 and Yukawa-21 at the Yukawa Institute for Theoretical Physics, Kyoto University. This work was supported by JSPS KAKENHI (Grants No. JP18H01876, No. JP21H01817, No. JP19H05823, No. JP20K05314, and No. JP22H01961).

APPENDIX A: QUASICLASSICAL THEORY IN THE STRONG SPIN-ORBIT COUPLING LIMIT

In the band basis representation, only the Zeeman field should be viewed as a perturbation, as opposed to previous studies on Rashba [62] (resp. multilayered Rashba [41,53]) superconductors, where the ASOC and the impurity self-energy (resp. the ASOC and Zeeman field) were treated as perturbations. One may integrate the 4×4 Green's function in 2×2 Nambu space and 2×2 spin space $\check{G}_l(i\omega_n, \mathbf{k}) = \check{G}_l(i\omega_n, \tilde{\mathbf{k}}, \xi_k^l)$ with respect to ξ_k^l instead of ξ_k for significantly split FSs I and II, respectively:

$$\begin{aligned} \check{g}_l(i\omega_n, \tilde{\mathbf{k}}) &\equiv \check{\tau}_3 \oint d\xi_k^l \begin{pmatrix} \hat{G}_l & \hat{F}_l \\ \hat{F}_l & \hat{G}_l \end{pmatrix}_{i\omega_n, \mathbf{k}} \\ &\equiv -i\pi \begin{pmatrix} \hat{g}_l & i\hat{f}_l \\ -i\hat{f}_l & -\hat{g}_l \end{pmatrix}_{i\omega_n, \tilde{\mathbf{k}}}, \end{aligned} \quad (\text{A1})$$

where $\tilde{\mathbf{k}}$ is the direction of the relative momentum and $\omega_n = (2n+1)\pi T$ is the Matsubara frequency for fermions. $\oint d\xi_k^l \dots$ indicates that the contributions from poles close to E_F for each split FS are taken into account.

The Eilenberger equation for spatially uniform systems, where $\nabla \check{g}_l = \check{\mathbf{0}}$, in the strong-ASOC regime is

$$[i\tilde{\omega}_n \check{\tau}_3 - \check{\Delta}_l(i\omega_n, \tilde{\mathbf{k}}) \pm \mu_B \check{g}_k^l \cdot \mathbf{H}, \check{g}_l(i\omega_n, \tilde{\mathbf{k}})] = \check{\mathbf{0}}, \quad (\text{A2})$$

$$\begin{aligned} \check{\Delta}_l(i\omega_n, \tilde{\mathbf{k}}) &= \begin{pmatrix} 0 & \tilde{\Delta}_l(i\omega_n, \tilde{\mathbf{k}}) \\ -\tilde{\Delta}_l^*(i\omega_n, \tilde{\mathbf{k}}) & 0 \end{pmatrix} \\ &\equiv \begin{pmatrix} 0 & \Delta_l(\tilde{\mathbf{k}}) + \sigma_l(i\omega_n) \\ -(\Delta_l^*(\tilde{\mathbf{k}}) + \bar{\sigma}_l(i\omega_n)) & 0 \end{pmatrix}, \end{aligned} \quad (\text{A3})$$

where $\tilde{\omega}_n \equiv \omega_n + \sigma_g(i\omega_n)$, $\Delta_l(\tilde{\mathbf{k}}) = \psi_s \pm d_l |\mathbf{g}_k^l|$, and $\check{g}_k^l = \text{diag}(\hat{g}_k^l, -\hat{g}_k^l)$ with $\hat{g}_k^l \equiv \mathbf{g}_k^l / |\mathbf{g}_k^l|$, and $+$ and $-$ correspond to $l = \text{I}$ and II , respectively. Assuming s -wave scattering in the Born limit, the nonmagnetic impurity scattering is incorporated through the self-energy [see Eqs. (B14) and (B20)]:

$$\sigma_g(i\omega_n) = \frac{\Gamma_n}{2} [(1+\delta)\langle g_{\text{I}}(i\omega_n, \tilde{\mathbf{k}}) \rangle_{\text{I}} + (1-\delta)\langle g_{\text{II}}(i\omega_n, \tilde{\mathbf{k}}) \rangle_{\text{II}}], \quad (\text{A4})$$

$$\sigma_{\text{I}}(i\omega_n) = \frac{\Gamma_n}{2} [(1+\delta)\langle f_{\text{I}}(i\omega_n, \tilde{\mathbf{k}}) \rangle_{\text{I}} + (1-\delta)\langle f_{\text{II}}(i\omega_n, \tilde{\mathbf{k}}) \rangle_{\text{II}}], \quad (\text{A5})$$

with $\langle \dots \rangle_l$ indicating an average over the FS l . Here, we used $g_{\text{I}} + \bar{g}_{\text{I}} = 0$, which holds for a spatially uniform system [40]. The solutions of the Eilenberger equation [Eq. (A2)] are readily obtained with the aid of the normalization condition $g_{\text{I}}^2 + f_{\text{I}} \bar{f}_{\text{I}} = 1$ as

$$g_{\text{I}}(i\omega_n, \tilde{\mathbf{k}}) = \pm (\tilde{\omega}_n \mp i\mu_B \bar{g}_k^l \cdot \mathbf{H}) / \Lambda_{\text{I}}(i\omega_n, \tilde{\mathbf{k}}), \quad (\text{A6})$$

$$f_{\text{I}}(i\omega_n, \tilde{\mathbf{k}}) = \pm \tilde{\Delta}_{\text{I}}(\tilde{\mathbf{k}}) / \Lambda_{\text{I}}(i\omega_n, \tilde{\mathbf{k}}), \quad (\text{A7})$$

with $\Lambda_{\text{I}}(i\omega_n, \tilde{\mathbf{k}}) \equiv \sqrt{(\tilde{\omega}_n \mp i\mu_B \bar{g}_k^l \cdot \mathbf{H})^2 + |\tilde{\Delta}_{\text{I}}(\tilde{\mathbf{k}})|^2}$. To satisfy the non-negativity of the real part of the retarded Green's function, which is directly related to the DOS,

$$\text{Re}[g_{\text{I}}(i\omega_n \rightarrow \mp i\mu_B \bar{g}_k^l \cdot \mathbf{H} + i\eta)] \geq 0, \quad (\text{A8})$$

we note that the sign in front of the Green's function for a uniform system can be set to coincide with $\text{sgn}[\text{Re}(\tilde{\omega}_n)]$ (see also [63]). Here, $\eta > 0$ is used for energy smearing.

APPENDIX B: NONMAGNETIC SCATTERING IN SPATIALLY UNIFORM NONCENTROSYMMETRIC SUPERCONDUCTORS

1. Eilenberger equation

The quasiclassical Green's function

$$\check{g}(\mathbf{r}, \tilde{\mathbf{k}}, i\omega_n) = -i\pi \begin{pmatrix} \hat{g} & i\hat{f} \\ -i\hat{f} & -\hat{g} \end{pmatrix} \quad (\text{B1})$$

follows the Eilenberger equation. In the case of the isotropic Rashba-type ASOC in the 2D system $[\mathbf{g}_{\tilde{\mathbf{k}}} = |\mathbf{g}_{\tilde{\mathbf{k}}}|(-\sin\phi, \cos\phi)]$, the equation in the presence of disorder is

$$\begin{aligned} i\mathbf{v}_F(\tilde{\mathbf{k}}) \cdot \nabla \check{g}(\mathbf{r}, \tilde{\mathbf{k}}, i\omega_n) \\ + [i\omega_n \check{\tau}_3 - \check{\Delta} - \check{\Sigma} - \alpha \check{g}_{\tilde{\mathbf{k}}} \cdot \check{\mathbf{S}}, \check{g}(\mathbf{r}, \tilde{\mathbf{k}}, i\omega_n)] = \check{\mathbf{0}}, \end{aligned} \quad (\text{B2})$$

with $\check{\tau}_3 = \text{diag}(\hat{\sigma}_0, -\hat{\sigma}_0)$, $\check{g}_{\tilde{\mathbf{k}}} = \text{diag}(\mathbf{g}_{\tilde{\mathbf{k}}} \hat{\sigma}_0, \mathbf{g}_{-\tilde{\mathbf{k}}} \hat{\sigma}_0)$, $\check{\mathbf{S}} = \text{diag}(\hat{\sigma}, \hat{\sigma}^\top)$, $\hat{\sigma}^\top = -\hat{\sigma}_y \hat{\sigma} \hat{\sigma}_y$,

$$\check{\Delta} = \begin{pmatrix} \hat{\mathbf{0}} & \hat{\Delta}(\mathbf{r}, \tilde{\mathbf{k}}) \\ -\hat{\Delta}^\dagger(\mathbf{r}, \tilde{\mathbf{k}}) & \hat{\mathbf{0}} \end{pmatrix}, \quad (\text{B3})$$

$$\hat{\Delta}(\mathbf{r}, \tilde{\mathbf{k}}) = [\psi_s(\mathbf{r}) \hat{\sigma}_0 + \mathbf{d}_{\tilde{\mathbf{k}}}(\mathbf{r}) \cdot \hat{\sigma}] i\hat{\sigma}_y, \quad (\text{B4})$$

$$\mathbf{d}_{\tilde{\mathbf{k}}}(\mathbf{r}) = d_{\tilde{\mathbf{k}}}(\mathbf{r}) \mathbf{g}_{\tilde{\mathbf{k}}} \quad (\text{B5})$$

as the order parameter, and $\check{\Sigma}(i\omega_n, \mathbf{r}, \tilde{\mathbf{k}}) \equiv \{\check{\Sigma}_{ij}\}_{i,j=1,2}$ as the impurity self-energy. The Eilenberger equation with respect to each component in Nambu space is recast as

$$\begin{aligned} \partial \hat{g}_0 + i\alpha \mathbf{g}_k \cdot (\hat{\sigma} \hat{g}_0 - \hat{g}_0 \hat{\sigma}) + i\hat{\Sigma}_{11}^0 \hat{g}_0 - i\hat{g}_0 \hat{\Sigma}_{11}^0 \\ + (\hat{\Delta}_0 + \hat{\Sigma}_{12}^0) \hat{f}_0 - \hat{f}_0 (\hat{\Delta}_0^\dagger - \hat{\Sigma}_{21}^0) = \hat{\mathbf{0}}, \end{aligned} \quad (\text{B6a})$$

$$\begin{aligned} \partial \hat{f}_0 + 2\omega_n \hat{f}_0 + i\alpha \mathbf{g}_k \cdot (\hat{\sigma} \hat{f}_0 - \hat{f}_0 \hat{\sigma}) + i\hat{\Sigma}_{11}^0 \hat{f}_0 + i\hat{f}_0 \hat{\Sigma}_{22}^0 \\ + (\hat{\Delta}_0 + \hat{\Sigma}_{12}^0) \hat{g}_0 - \hat{g}_0 (\hat{\Delta}_0 + \hat{\Sigma}_{12}^0) = \hat{\mathbf{0}}, \end{aligned} \quad (\text{B6b})$$

$$\begin{aligned} \partial \hat{f}_0 - 2\omega_n \hat{f}_0 + i\alpha \mathbf{g}_k \cdot (\hat{\sigma} \hat{f}_0 - \hat{f}_0 \hat{\sigma}) - i\hat{\Sigma}_{22}^0 \hat{f}_0 - i\hat{f}_0 \hat{\Sigma}_{11}^0 \\ + (\hat{\Delta}_0^\dagger - \hat{\Sigma}_{21}^0) \hat{g}_0 - \hat{g}_0 (\hat{\Delta}_0^\dagger - \hat{\Sigma}_{21}^0) = \hat{\mathbf{0}}, \end{aligned} \quad (\text{B6c})$$

$$\begin{aligned} \partial \hat{g}_0 + i\alpha \mathbf{g}_k \cdot (\hat{\sigma} \hat{g}_0 - \hat{g}_0 \hat{\sigma}) - i\hat{\Sigma}_{22}^0 \hat{g}_0 + i\hat{g}_0 \hat{\Sigma}_{22}^0 \\ + (\hat{\Delta}_0^\dagger - \hat{\Sigma}_{21}^0) \hat{f}_0 - \hat{f}_0 (\hat{\Delta}_0 + \hat{\Sigma}_{12}^0) = \hat{\mathbf{0}}, \end{aligned} \quad (\text{B6d})$$

with the normalization conditions

$$\hat{g}_0^2 + \hat{f}_0 \hat{f}_0 = \hat{\sigma}_0, \quad (\text{B7a})$$

$$\hat{g}_0 \hat{f}_0 + \hat{f}_0 \hat{g}_0 = \hat{\mathbf{0}}, \quad (\text{B7b})$$

$$\hat{f}_0 \hat{g}_0 + \hat{g}_0 \hat{f}_0 = \hat{\mathbf{0}}, \quad (\text{B7c})$$

$$\hat{f}_0 \hat{f}_0 + \hat{g}_0^2 = \hat{\sigma}_0, \quad (\text{B7d})$$

where we define $\partial \equiv \mathbf{v}_F \cdot \nabla$, $\hat{g} \equiv \hat{g}_0$, $\hat{f} \equiv \hat{f}_0 i\hat{\sigma}_y$, $\hat{f}^\dagger \equiv -i\hat{\sigma}_y \hat{f}_0$, $\hat{g}^\dagger \equiv -\hat{\sigma}_y \hat{g}_0 \hat{\sigma}_y$, $\hat{\Sigma}_{11} \equiv \hat{\Sigma}_{11}^0$, $\hat{\Sigma}_{12} \equiv \hat{\Sigma}_{12}^0 i\hat{\sigma}_y$, $\hat{\Sigma}_{21} \equiv -i\hat{\sigma}_y \hat{\Sigma}_{21}^0$, $\hat{\Sigma}_{22} \equiv -\hat{\sigma}_y \hat{\Sigma}_{22}^0 \hat{\sigma}_y$, $\hat{\Delta} \equiv \hat{\Delta}_0 i\hat{\sigma}_y$, and $\hat{\Delta}^\dagger \equiv -i\hat{\sigma}_y \hat{\Delta}_0^\dagger$.

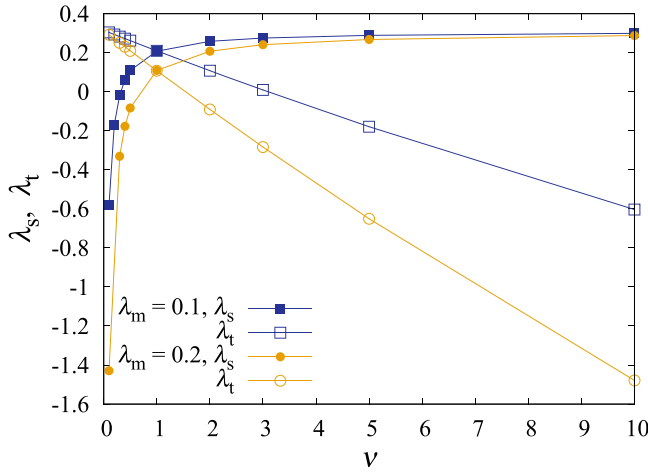


FIG. 7. Mixing ratio dependence of the coupling constants for the singlet and triplet channels evaluated for Si(111)- $(\sqrt{7} \times \sqrt{3})$ -In. The DOS difference between the split FSs is set to $\delta = 0$.

2. Impurity self-energy in the Born limit

We next describe the nonmagnetic impurity scattering in a spatially uniform Rashba system. We assume s -wave scattering in the Born limit. The self-energy due to the nonmagnetic impurity scattering for split FSs is given by

$$\check{\Sigma}_{I,II}(\omega_n) = \frac{\Gamma_n}{\pi} \langle \check{g}_{I,II}(\omega_n, \vec{k}) \rangle_{I,II}, \quad (\text{B8})$$

where $\Gamma_n = \pi n_{\text{imp}} N_F v^2$ is the impurity scattering rate in the normal state, n_{imp} is the density of impurities, $N_F = (N_I + N_{II})/2$ is the DOS at the Fermi level in the normal state, and v is the s -wave scattering potential of an impurity.

We can separate the Green's functions with respect to each split band due to the ASOC using the band basis where the normal-state Hamiltonian is diagonal (see the Appendix of Ref. [40]), at least in the case of spatially uniform systems [39] or spatially inhomogeneous systems within the clean limit (e.g., clean vortex states) [64].

Transformation of the Green's functions into the orbital basis (where the spin quantization axis is parallel to an applied field) then yields [39,40,64]

$$\hat{g} = g_I \hat{\sigma}_I + g_{II} \hat{\sigma}_{II}, \quad (\text{B9a})$$

$$\hat{f} = (f_I \hat{\sigma}_I + f_{II} \hat{\sigma}_{II}) i \hat{\sigma}_y, \quad (\text{B9b})$$

$$\hat{f} = -i \hat{\sigma}_y (\bar{f}_I \hat{\sigma}_I + \bar{f}_{II} \hat{\sigma}_{II}), \quad (\text{B9c})$$

$$\hat{g} = -\hat{\sigma}_y (\bar{g}_I \hat{\sigma}_I + \bar{g}_{II} \hat{\sigma}_{II}) i \hat{\sigma}_y, \quad (\text{B9d})$$

where $\hat{\sigma}_{I,II} = (\hat{\sigma}_0 \pm \bar{\mathbf{g}}_{\vec{k}} \cdot \hat{\boldsymbol{\sigma}})/2$ and $\bar{\mathbf{g}}_{\vec{k}} \equiv \mathbf{g}_{\vec{k}}/|\mathbf{g}_{\vec{k}}|$. Provided that the Green's functions are invariant under the transformation $\vec{k} \rightarrow -\vec{k}$ [65], we obtain

$$\langle \hat{g} \rangle_{\vec{k}} = \frac{1}{2} \langle g_I + g_{II} \rangle_{\vec{k}} \hat{\sigma}_0, \quad (\text{B10a})$$

$$\langle \hat{f} \rangle_{\vec{k}} = \frac{1}{2} \langle f_I + f_{II} \rangle_{\vec{k}} \hat{\sigma}_0 i \hat{\sigma}_y, \quad (\text{B10b})$$

$$\langle \hat{f} \rangle_{\vec{k}} = -i \hat{\sigma}_y \frac{1}{2} \langle \bar{f}_I + \bar{f}_{II} \rangle_{\vec{k}} \hat{\sigma}_0, \quad (\text{B10c})$$

$$\langle \hat{g} \rangle_{\vec{k}} = -\hat{\sigma}_y \frac{1}{2} \langle \bar{g}_I + \bar{g}_{II} \rangle_{\vec{k}} \hat{\sigma}_0 i \hat{\sigma}_y, \quad (\text{B10d})$$

because $\bar{\mathbf{g}}_{-\vec{k}} = -\bar{\mathbf{g}}_{\vec{k}}$. Thus,

$$\langle \hat{g}_0 \rangle_{\vec{k}} = \frac{1}{2} \langle g_I + g_{II} \rangle_{\vec{k}} \hat{\sigma}_0, \quad (\text{B11a})$$

$$\langle \hat{f}_0 \rangle_{\vec{k}} = \frac{1}{2} \langle f_I + f_{II} \rangle_{\vec{k}} \hat{\sigma}_0, \quad (\text{B11b})$$

$$\langle \hat{f}_0 \rangle_{\vec{k}} = \frac{1}{2} \langle \bar{f}_I + \bar{f}_{II} \rangle_{\vec{k}} \hat{\sigma}_0, \quad (\text{B11c})$$

$$\langle \hat{g}_0 \rangle_{\vec{k}} = \frac{1}{2} \langle \bar{g}_I + \bar{g}_{II} \rangle_{\vec{k}} \hat{\sigma}_0. \quad (\text{B11d})$$

Therefore,

$$\hat{\Sigma}_{11}^0 = -i \Gamma_n \langle \hat{g}_0 \rangle_{\vec{k}} = -i \Gamma_n \frac{1}{2} \langle g_I + g_{II} \rangle_{\vec{k}} \hat{\sigma}_0, \quad (\text{B12a})$$

$$\hat{\Sigma}_{12}^0 = \Gamma_n \langle \hat{f}_0 \rangle_{\vec{k}} = \Gamma_n \frac{1}{2} \langle f_I + f_{II} \rangle_{\vec{k}} \hat{\sigma}_0, \quad (\text{B12b})$$

$$\hat{\Sigma}_{21}^0 = -\Gamma_n \langle \hat{f}_0 \rangle_{\vec{k}} = -\Gamma_n \frac{1}{2} \langle \bar{f}_I + \bar{f}_{II} \rangle_{\vec{k}} \hat{\sigma}_0, \quad (\text{B12c})$$

$$\hat{\Sigma}_{22}^0 = i \Gamma_n \langle \hat{g}_0 \rangle_{\vec{k}} = i \Gamma_n \frac{1}{2} \langle \bar{g}_I + \bar{g}_{II} \rangle_{\vec{k}} \hat{\sigma}_0. \quad (\text{B12d})$$

We note that, in the case of a spatially uniform system, the impurity self-energies $\hat{\Sigma}_{ij}^0$ are proportional to the unit matrix $\hat{\sigma}_0$.

Using Eqs. (B12a)–(B12d), in the Eilenberger equations (B6a), (B6b), (B6c), and (B6d), respectively, we obtain

$$i \hat{\Sigma}_{11}^0 \hat{g}_0 - i \hat{g}_0 \hat{\Sigma}_{11}^0 = \hat{0}, \quad (\text{B13a})$$

$$2\omega_n \hat{f}_0 + i \hat{\Sigma}_{11}^0 \hat{f}_0 + i \hat{f}_0 \hat{\Sigma}_{22}^0 = 2(\omega_n + \sigma_g) \hat{\sigma}_0 \hat{f}_0, \quad (\text{B13b})$$

$$-2\omega_n \hat{f}_0 - i \hat{\Sigma}_{22}^0 \hat{f}_0 - i \hat{f}_0 \hat{\Sigma}_{11}^0 = -2(\omega_n + \sigma_g) \hat{\sigma}_0 \hat{f}_0, \quad (\text{B13c})$$

$$-i \hat{\Sigma}_{22}^0 \hat{g}_0 + i \hat{g}_0 \hat{\Sigma}_{22}^0 = \hat{0}, \quad (\text{B13d})$$

where

$$\begin{aligned} \sigma_g &\equiv \frac{\Gamma_n}{2} (1 + \delta) \frac{1}{2} \langle (g_I - \bar{g}_I) \rangle_{\vec{k}} + \frac{\Gamma_n}{2} (1 - \delta) \frac{1}{2} \langle (g_{II} - \bar{g}_{II}) \rangle_{\vec{k}} \\ &= \frac{\Gamma_n}{2} (1 + \delta) \langle g_I \rangle_{\vec{k}} + \frac{\Gamma_n}{2} (1 - \delta) \langle g_{II} \rangle_{\vec{k}}. \end{aligned} \quad (\text{B14})$$

In the spatially uniform system, we may use $g_{I,II} + \bar{g}_{I,II} = 0$ to get Eq. (B14). The parameter $\delta = (N_I - N_{II})/2N_F$ ($-1 < \delta < 1$) characterizes the difference in the DOSs between the split FSs I and II. In the Eilenberger equations (B6a)–(B6d), the rotation in spin space represented by the unitary matrix $\hat{U}_{\vec{k}}$ yields

$$\hat{U}_{\vec{k}}^\dagger i \alpha \mathbf{g}_{\vec{k}} \cdot (\hat{\boldsymbol{\sigma}} \hat{A}_0 - \hat{A}_0 \hat{\boldsymbol{\sigma}}) \hat{U}_{\vec{k}} = 2i \alpha |\mathbf{g}_{\vec{k}}| \begin{pmatrix} 0 & -A_b \\ A_c & 0 \end{pmatrix}, \quad (\text{B15})$$

$$\hat{U}_{\vec{k}}^\dagger (\hat{\Delta}_0 + \hat{\Sigma}_{12}^0) \hat{U}_{\vec{k}} = \begin{pmatrix} \Delta_{II} + \sigma_f & 0 \\ 0 & \Delta_I + \sigma_f \end{pmatrix}, \quad (\text{B16})$$

$$\hat{U}_{\vec{k}}^\dagger (\hat{\Delta}_0^\dagger - \hat{\Sigma}_{21}^0) \hat{U}_{\vec{k}} = \begin{pmatrix} \Delta_{II}^* + \bar{\sigma}_f & 0 \\ 0 & \Delta_I^* + \bar{\sigma}_f \end{pmatrix}, \quad (\text{B17})$$

where \hat{A}_0 refers to \hat{g}_0 , \hat{f}_0 , \hat{f}_0 , or \hat{g}_0 and

$$\hat{U}_{\vec{k}}^\dagger \hat{A}_0 \hat{U}_{\vec{k}} \equiv \begin{pmatrix} A_a & A_b \\ A_c & A_d \end{pmatrix}, \quad (\text{B18})$$

$$\Delta_{I,II} \equiv \psi_s \pm d_I |\mathbf{g}_{\vec{k}}|, \quad (\text{B19})$$

$$\sigma_f \equiv \Gamma_n (1 + \delta) \frac{1}{2} \langle f_I \rangle_{\vec{k}} + \Gamma_n (1 - \delta) \frac{1}{2} \langle f_{II} \rangle_{\vec{k}}, \quad (\text{B20})$$

$$\bar{\sigma}_f \equiv \Gamma_n (1 + \delta) \frac{1}{2} \langle \bar{f}_I \rangle_{\vec{k}} + \Gamma_n (1 - \delta) \frac{1}{2} \langle \bar{f}_{II} \rangle_{\vec{k}}. \quad (\text{B21})$$

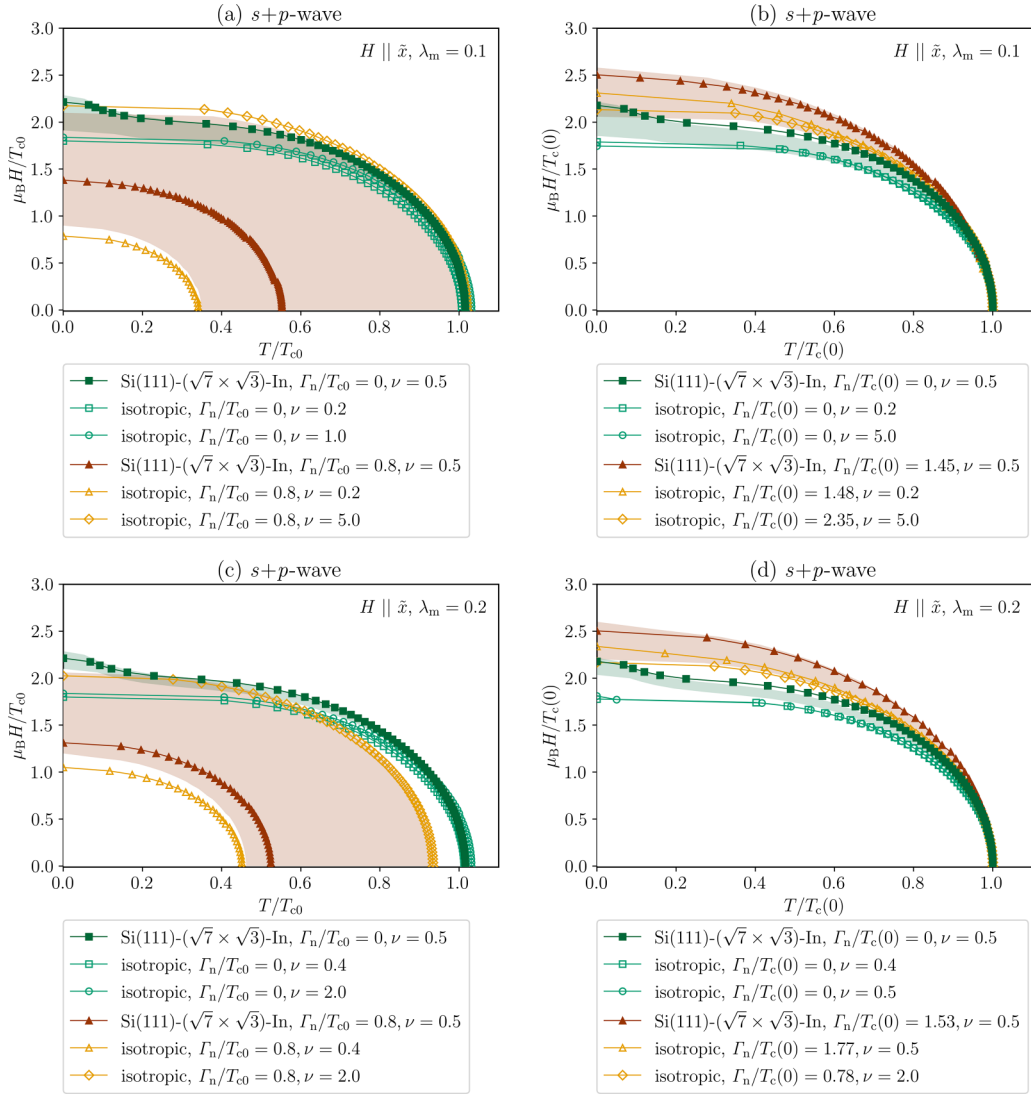


FIG. 8. Temperature dependence of an in-plane critical magnetic field oriented parallel to the x axis for the $s + p$ -wave pairing upon changing the normal state scattering rate Γ_n and the parity-mixing ratio ν for (a), (b) $\lambda_m = 0.1$ and (c), (d) $\lambda_m = 0.2$. The filled and open symbols denote the data for the Fermi surface of a Si(111)-($\sqrt{7} \times \sqrt{3}$)-In and an isotropic system, respectively. The difference of the density of states between the split two FSs is set to $\delta = 0$. Temperature and magnetic field are normalized by (a), (c) T_{c0} and (b), (d) $T_c(0)$, respectively.

Hence, the impurity effect in the spatially uniform state appears only in the replacement of the Matsubara frequency and the order parameter:

$$\omega_n \rightarrow \tilde{\omega}_n \equiv \omega_n + \sigma_g, \quad (\text{B22})$$

$$\Delta_{I,II} \rightarrow \tilde{\Delta}_{I,II} \equiv \Delta_{I,II} + \sigma_f, \quad (\text{B23})$$

$$\Delta_{I,II}^* \rightarrow \tilde{\Delta}_{I,II}^* \equiv \Delta_{I,II}^* + \bar{\sigma}_f. \quad (\text{B24})$$

3. Gap equation

In the same manner as Ref. [40], we obtain the following Eilenberger equations in the band basis in the presence of impurities for the suffix a:

$$\tilde{\Delta}_{II} \bar{f}_a - \tilde{\Delta}_{II}^* f_a = 0, \quad (\text{B25a})$$

$$2\tilde{\omega}_n f_a + \tilde{\Delta}_{II} \bar{g}_a - \tilde{\Delta}_{II} g_a = 0, \quad (\text{B25b})$$

$$2\tilde{\omega}_n \bar{f}_a - \tilde{\Delta}_{II}^* g_a + \tilde{\Delta}_{II}^* \bar{g}_a = 0, \quad (\text{B25c})$$

$$\tilde{\Delta}_{II}^* f_a - \tilde{\Delta}_{II} \bar{f}_a = 0. \quad (\text{B25d})$$

For the suffix b, we obtain

$$-2i\alpha |g_{\mathbf{k}}| g_b + \tilde{\Delta}_{II} \bar{f}_b - \tilde{\Delta}_I^* f_b = 0, \quad (\text{B26a})$$

$$2\tilde{\omega}_n f_b - 2i\alpha |g_{\mathbf{k}}| f_b + \tilde{\Delta}_{II} \bar{g}_b - \tilde{\Delta}_I g_b = 0, \quad (\text{B26b})$$

$$2\tilde{\omega}_n \bar{f}_b + 2i\alpha |g_{\mathbf{k}}| \bar{f}_b - \tilde{\Delta}_{II}^* g_b + \tilde{\Delta}_I^* \bar{g}_b = 0, \quad (\text{B26c})$$

$$-2i\alpha |g_{\mathbf{k}}| \bar{g}_b + \tilde{\Delta}_{II}^* f_b - \tilde{\Delta}_I \bar{f}_b = 0. \quad (\text{B26d})$$

For the suffix c, we obtain

$$2i\alpha |g_{\mathbf{k}}| g_c + \tilde{\Delta}_I \bar{f}_c - \tilde{\Delta}_{II}^* f_c = 0, \quad (\text{B27a})$$

$$2\tilde{\omega}_n f_c + 2i\alpha |g_{\mathbf{k}}| f_c + \tilde{\Delta}_I \bar{g}_c - \tilde{\Delta}_{II} g_c = 0, \quad (\text{B27b})$$

$$2\tilde{\omega}_n \bar{f}_c - 2i\alpha |g_{\mathbf{k}}| \bar{f}_c - \tilde{\Delta}_I^* g_c + \tilde{\Delta}_{II}^* \bar{g}_c = 0, \quad (\text{B27c})$$

$$2i\alpha |g_{\mathbf{k}}| \bar{g}_c + \tilde{\Delta}_I^* f_c - \tilde{\Delta}_{II} \bar{f}_c = 0. \quad (\text{B27d})$$

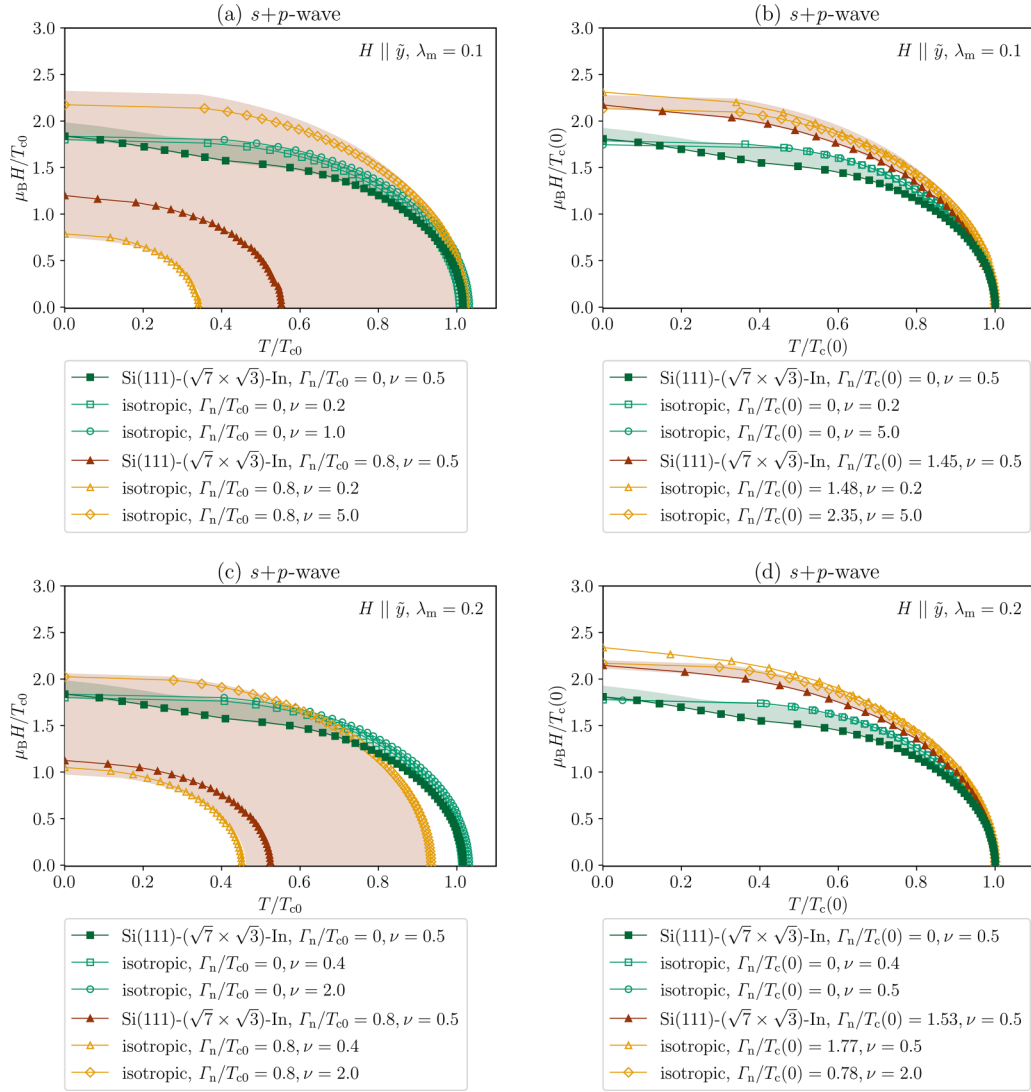


FIG. 9. Temperature dependence of an in-plane critical magnetic field oriented parallel to the y axis for the $s + p$ -wave pairing upon changing the normal state scattering rate Γ_n and the parity-mixing ratio ν for (a), (b) $\lambda_m = 0.1$ and (c), (d) $\lambda_m = 0.2$. The filled and open symbols denote the data for the Fermi surface of a $\text{Si}(111)-(\sqrt{7} \times \sqrt{3})\text{-In}$ and an isotropic system, respectively. The difference of the density of states between the split two FSs is set to $\delta = 0$. Temperature and magnetic field are normalized by (a), (c) T_{c0} and (b), (d) $T_c(0)$, respectively.

Finally, for the suffix d, we obtain

$$\tilde{\Delta}_I \tilde{f}_d - \tilde{\Delta}_I^* f_d = 0, \quad (\text{B28a})$$

$$2\tilde{\omega}_n f_d + \tilde{\Delta}_I \tilde{g}_d - \tilde{\Delta}_I g_d = 0, \quad (\text{B28b})$$

$$2\tilde{\omega}_n \tilde{f}_d - \tilde{\Delta}_I^* g_d + \tilde{\Delta}_I^* \tilde{g}_d = 0, \quad (\text{B28c})$$

$$\tilde{\Delta}_I^* f_d - \tilde{\Delta}_I \tilde{f}_d = 0. \quad (\text{B28d})$$

As discussed in Ref. [40], we note that $g_{b,c} = f_{b,c} = \tilde{f}_{b,c} = \tilde{g}_{b,c} = 0$ for $\alpha |g_{\tilde{k}}| \neq 0$. However, as opposed to the clean-limit case, this result is valid only for spatially uniform systems. By transforming the normalization condition (B7b) or (B7c) into that in the band basis, we obtain $g_{a,d} = -\tilde{g}_{a,d}$ for spatially uniform systems. From this relation, the normalization

condition (B7a), and the Eilenberger equations (B25) and (B28), we obtain the following Green's functions for spatially uniform systems:

$$g_{d,a} \equiv g_{I,\Pi}(i\omega_n, \tilde{\mathbf{k}}) = \frac{\omega_n + \sigma_g(i\omega_n)}{\Lambda_{I,\Pi}(i\omega_n, \tilde{\mathbf{k}})}, \quad (\text{B29a})$$

$$f_{d,a} \equiv f_{I,\Pi}(i\omega_n, \tilde{\mathbf{k}}) = \frac{\Delta_{I,\Pi}(\tilde{\mathbf{k}}) + \sigma_f(i\omega_n)}{\Lambda_{I,\Pi}(i\omega_n, \tilde{\mathbf{k}})}, \quad (\text{B29b})$$

$$\tilde{f}_{d,a} \equiv \tilde{f}_{I,\Pi}(i\omega_n, \tilde{\mathbf{k}}) = \frac{\Delta_{I,\Pi}^*(\tilde{\mathbf{k}}) + \bar{\sigma}_f(i\omega_n)}{\Lambda_{I,\Pi}(i\omega_n, \tilde{\mathbf{k}})}, \quad (\text{B29c})$$

$$\tilde{g}_{d,a} \equiv \tilde{g}_{I,\Pi}(i\omega_n, \tilde{\mathbf{k}}) = \frac{-\omega_n - \sigma_g(i\omega_n)}{\Lambda_{I,\Pi}(i\omega_n, \tilde{\mathbf{k}})}, \quad (\text{B29d})$$

where $\Lambda_{I,II}(i\omega_n, \vec{k}) = \sqrt{\tilde{\omega}_n^2 + |\tilde{\Delta}_{I,II}|^2}$. The corresponding gap equations are

$$\psi_s = \pi T \sum_{|\omega_n| < \omega_c} [\lambda_s \{ \langle f_+ \rangle_0 + \delta \langle f_- \rangle_0 \} + \lambda_m \{ \langle |\mathbf{g}_{\vec{k}}| f_- \rangle_0 + \delta \langle |\mathbf{g}_{\vec{k}}| f_+ \rangle_0 \}], \quad (\text{B30})$$

$$d_t = \pi T \sum_{|\omega_n| < \omega_c} [\lambda_t \{ \langle |\mathbf{g}_{\vec{k}}| f_- \rangle_0 + \delta \langle |\mathbf{g}_{\vec{k}}| f_+ \rangle_0 \} + \lambda_m \{ \langle f_+ \rangle_0 + \delta \langle f_- \rangle_0 \}], \quad (\text{B31})$$

where $f_{\pm} \equiv (f_I + f_{II})/2$ and ω_c is the cutoff frequency. In the clean limit and in the limit of $T \rightarrow T_c$, the coupling constants are determined as follows [40]:

$$\lambda_s = \frac{\lambda\nu - \lambda_m(1 + \delta\nu \langle |\mathbf{g}_{\vec{k}}| \rangle_0)}{\nu + \delta \langle |\mathbf{g}_{\vec{k}}| \rangle_0}, \quad (\text{B32})$$

$$\lambda_t = \frac{\lambda - \lambda_m(\nu + \delta \langle |\mathbf{g}_{\vec{k}}| \rangle_0)}{1 + \delta\nu \langle |\mathbf{g}_{\vec{k}}| \rangle_0}. \quad (\text{B33})$$

Here, ν , λ , and $n_c(T)$ are defined in the main text.

APPENDIX C: $H_{c2}^{\parallel}(T)$ VARIATION WITH PARITY MIXING

To study the variation of $H_{c2}^{\parallel}(T)$ when ν changes over a wide range, it turned out that the coupling constant for the mixing channel is limited to $\lambda_m \ll 1$. This is because the self-consistent solutions of the order parameter can be obtained only when $-0.2 \lesssim \lambda_s, \lambda_t \lesssim 0.3$ (see Fig. 7), suggesting that the variation range of ν narrows as λ_m increases. Therefore,

we will limit ourselves to $\lambda_m = 0.1$ and 0.2 . Figure 7 shows the dependence of the coupling constants λ_s and λ_t on ν evaluated by Eqs. (3.6) and (3.7) for Si(111)-($\sqrt{7} \times \sqrt{3}$)-In. The coupling constants are controlled by the input parameters λ_m and ν . At the equal-mixing ratio ($\nu = 1$), $\lambda_s \approx \lambda_t$ for $\lambda_m = 0.1$ and 0.2 , respectively. For $\lambda_m = 0.1$, the self-consistent solution of the order parameter was not obtained for $\nu = 0.1$ and 10 , while for $\lambda_m = 0.2$, it was not obtained for $\nu \lesssim 0.3$ or $\nu \gtrsim 3$. We consider that the choice of $\lambda_m = 0.1$ and 0.2 is reasonable, since these values correspond to the weak-coupling regime.

In Figs. 8 and 9, we show the $H_{c2}^{\parallel}(T)$ oriented parallel to the x and y axes, respectively, in the case of the $s + p$ -wave pairing to check the stability of the results in Figs. 3 and 4, respectively, upon changing ν and λ_m . The physical quantities are rescaled by $T_c(0)$ in Figs. 8(b), 8(d), 9(b), and 9(d). The green and red shaded areas in Figs. 8 and 9 depict the variation range of the transition line when ν varies in the case of $\Gamma_n/T_{c0} = 0$ and 0.8 , respectively, for Si(111)-($\sqrt{7} \times \sqrt{3}$)-In. For an isotropic FS, the variation range of H_{c2}^{\parallel} is shown by the area between open symbols. For $\lambda_m = 0.1$ (0.2), we varied ν in the range $0.2 \leq \nu \leq 5$ ($0.4 \leq \nu \leq 2$) in any conditions to show the variation of the transition line such that the variation of $H_{c2}^{\parallel}(0)$ is the largest.

Figure 8 shows the same trend of $H_{c2}^{\parallel}(T \approx 0)$ for Si(111)-($\sqrt{7} \times \sqrt{3}$)-In being larger than that for isotropic systems as in Fig. 3. Figure 9 also shows the same trend of the suppression of the $H_{c2}^{\parallel}(T \approx 0)$ enhancement as in Fig. 4, although it shows some variation depending on ν .

-
- [1] Y. Saito, T. Nojima, and Y. Iwasa, Highly crystalline 2D superconductors, *Nat. Rev. Mater.* **2**, 16094 (2016).
- [2] T. Uchihashi, Two-dimensional superconductors with atomic-scale thickness, *Supercond. Sci. Technol.* **30**, 013002 (2017).
- [3] D. V. Gruznev, A. V. Zotov, and A. A. Saranin, One-atom-layer compounds on silicon and germanium, *Jpn. J. Appl. Phys.* **56**, 08LA01 (2017).
- [4] M. Strongin, R. S. Thompson, O. F. Kammerer, and J. E. Crow, Destruction of superconductivity in disordered near-monolayer films, *Phys. Rev. B* **1**, 1078 (1970).
- [5] H. M. Jaeger, D. B. Haviland, A. M. Goldman, and B. G. Orr, Threshold for superconductivity in ultrathin amorphous gallium films, *Phys. Rev. B* **34**, 4920 (1986).
- [6] D. B. Haviland, Y. Liu, and A. M. Goldman, Onset of Superconductivity in the Two-Dimensional Limit, *Phys. Rev. Lett.* **62**, 2180 (1989).
- [7] T. Sekihara, R. Masutomi, and T. Okamoto, Two-Dimensional Superconducting State of Monolayer Pb Films Grown on GaAs(110) in a Strong Parallel Magnetic Field, *Phys. Rev. Lett.* **111**, 057005 (2013).
- [8] T. Sekihara, T. Miyake, R. Masutomi, and T. Okamoto, Effect of Parallel Magnetic Field on Superconductivity of Ultrathin Metal Films Grown on a Cleaved GaAs Surface, *J. Phys. Soc. Jpn.* **84**, 064710 (2015).
- [9] T. Zhang, P. Cheng, W.-J. Li, Y.-J. Sun, G. Wang, X.-G. Zhu, K. He, L. Wang, X. Ma, X. Chen *et al.*, Superconductivity in one-atomic-layer metal films grown on Si(111), *Nat. Phys.* **6**, 104 (2010).
- [10] T. Uchihashi, P. Mishra, M. Aono, and T. Nakayama, Macroscopic Superconducting Current through a Silicon Surface Reconstruction with Indium Adatoms: Si(111)-($\sqrt{7} \times \sqrt{3}$)-In, *Phys. Rev. Lett.* **107**, 207001 (2011).
- [11] A. V. Matetskiy, S. Ichinokura, L. V. Bondarenko, A. Y. Tupchaya, D. V. Gruznev, A. V. Zotov, A. A. Saranin, R. Hobar, A. Takayama, and S. Hasegawa, Two-Dimensional Superconductor with a Giant Rashba Effect: One-Atom-Layer TI-Pb Compound on Si(111), *Phys. Rev. Lett.* **115**, 147003 (2015).
- [12] Y. Wu, M.-C. Duan, N. Liu, G. Yao, D. Guan, S. Wang, Y.-Y. Li, H. Zheng, C. Liu, and J.-F. Jia, Diamagnetic response of a superconducting surface superstructure: Si(111)- $\sqrt{7} \times \sqrt{3}$ -In, *Phys. Rev. B* **99**, 140506(R) (2019).
- [13] L. Petersen and P. Hedegård, A simple tight-binding model of spin-orbit splitting of sp -derived surface states, *Surf. Sci.* **459**, 49 (2000).
- [14] J. Friedel, P. Lenglar, and G. Leman, Etude du couplage spin-orbite dans les metaux de transition: Application au platine, *J. Phys. Chem. Solids* **25**, 781 (1964).
- [15] R. Meservey and P. Tedrow, Spin-orbit scattering in superconducting thin films, *Phys. Lett. A* **58**, 131 (1976).
- [16] T. Uchihashi, Surface atomic-layer superconductors with Rashba/Zeeman-type spin-orbit coupling, *AAPPS Bull.* **31**, 27 (2021).

- [17] P. A. Frigeri, D. F. Agterberg, and M. Sigrist, Spin susceptibility in superconductors without inversion symmetry, *New J. Phys.* **6**, 115 (2004).
- [18] P. W. Anderson, Structure of “triplet” superconducting energy gaps, *Phys. Rev. B* **30**, 4000 (1984).
- [19] L. P. Gor’kov and E. I. Rashba, Superconducting 2D System with Lifted Spin Degeneracy: Mixed Singlet-Triplet State, *Phys. Rev. Lett.* **87**, 037004 (2001).
- [20] P. A. Frigeri, D. F. Agterberg, A. Koga, and M. Sigrist, Superconductivity without Inversion Symmetry: MnSi versus CePt₃Si, *Phys. Rev. Lett.* **92**, 097001 (2004).
- [21] D. V. Gruznev, L. V. Bondarenko, A. V. Matetskiy, A. A. Yakovlev, A. Y. Tupchaya, S. V. Eremeev, E. V. Chulkov, J.-P. Chou, C.-M. Wei, M.-Y. Lai *et al.*, A strategy to create spin-split metallic bands on silicon using a dense alloy layer, *Sci. Rep.* **4**, 4742 (2014).
- [22] E. Rotenberg, H. Koh, K. Rossnagel, H. W. Yeom, J. Schäfer, B. Krenzer, M. P. Rocha, and S. D. Kevan, Indium $\sqrt{7} \times \sqrt{3}$ on Si(111): A Nearly Free Electron Metal in Two Dimensions, *Phys. Rev. Lett.* **91**, 246404 (2003).
- [23] T. Kobayashi, Y. Nakata, K. Yaji, T. Shishidou, D. Agterberg, S. Yoshizawa, F. Komori, S. Shin, M. Weinert, T. Uchihashi, and K. Sakamoto, Orbital Angular Momentum Induced Spin Polarization of 2D Metallic Bands, *Phys. Rev. Lett.* **125**, 176401 (2020).
- [24] S. Yoshizawa, T. Kobayashi, Y. Nakata, K. Yaji, K. Yokota, F. Komori, S. Shin, K. Sakamoto, and T. Uchihashi, Atomic-layer Rashba-type superconductor protected by dynamic spin-momentum locking, *Nat. Commun.* **12**, 1462 (2021).
- [25] Y. Saito, Y. Nakamura, M. S. Bahramy, Y. Kohama, J. Ye, Y. Kasahara, Y. Nakagawa, M. Onga, M. Tokunaga, T. Nojima, Y. Yanase, and Y. Iwasa, Superconductivity protected by spin-valley locking in ion-gated MoS₂, *Nat. Phys.* **12**, 144 (2016).
- [26] E. I. Rashba, Svoistva poluprovodnikov s ekstremal’noi petlei. I. Tsiklotronnyi i kombinatsionnyi rezonans v magnitnom pole, perpendikulyarnom ploskosti petli, Fizika tverd. tela **2**, 1224 (1960) [Properties of semiconductors with an extremum loop. I. Cyclotron and combinational resonance in a magnetic field perpendicular to the plane of the loop, *Sov. Phys. Solid State* **2**, 1109 (1960)].
- [27] Yu. A. Bychkov and É. I. Rashba, Svoistva dvumernogo elektronogo gaza so snyatym vyrozhdeniem spektra, Pis’ma v ZhETF **39**, 66 (1984) [Properties of a 2D electron gas with lifted spectral degeneracy, *JETP Lett.* **39**, 78 (1984)].
- [28] L. N. Bulaevskii, Magnetic properties of layered superconductors with weak interaction between the layers, Zh. Eksp. Teor. Fiz. **64**, 2241 (1973) [*Sov. Phys. JETP* **37**, 1133 (1973)].
- [29] K. Maki, Effect of Pauli Paramagnetism on Magnetic Properties of High-Field Superconductors, *Phys. Rev.* **148**, 362 (1966).
- [30] O. V. Dimitrova and M. V. Feigel’man, Phase diagram of a surface superconductor in parallel magnetic field, *J. Exp. Theor. Phys. Lett.* **78**, 637 (2003).
- [31] O. Dimitrova and M. V. Feigel’man, Theory of a two-dimensional superconductor with broken inversion symmetry, *Phys. Rev. B* **76**, 014522 (2007).
- [32] K. V. Samokhin, Upper critical field in noncentrosymmetric superconductors, *Phys. Rev. B* **78**, 224520 (2008).
- [33] D. F. Agterberg and R. P. Kaur, Magnetic-field-induced helical and stripe phases in Rashba superconductors, *Phys. Rev. B* **75**, 064511 (2007).
- [34] Y. Yanase and M. Sigrist, Helical Superconductivity in Non-centrosymmetric Superconductors with Dominantly Spin Triplet Pairing, *J. Phys. Soc. Jpn.* **77**, 342 (2008).
- [35] G. Zwicknagl, S. Jahns, and P. Fulde, Critical magnetic field of ultra-thin superconducting films and interfaces, *J. Phys. Soc. Jpn.* **86**, 083701 (2017).
- [36] M. Houzet and J. S. Meyer, Quasiclassical theory of disordered Rashba superconductors, *Phys. Rev. B* **92**, 014509 (2015).
- [37] V. Barzykin and L. P. Gor’kov, Inhomogeneous Stripe Phase Revisited for Surface Superconductivity, *Phys. Rev. Lett.* **89**, 227002 (2002).
- [38] R. P. Kaur, D. F. Agterberg, and M. Sigrist, Helical Vortex Phase in the Noncentrosymmetric CePt₃Si, *Phys. Rev. Lett.* **94**, 137002 (2005).
- [39] P. A. Frigeri, D. F. Agterberg, I. Milat, and M. Sigrist, Phenomenological theory of the *s*-wave state in superconductors without an inversion center, *Eur. Phys. J. B* **54**, 435 (2006).
- [40] N. Hayashi, K. Wakabayashi, P. A. Frigeri, and M. Sigrist, Temperature dependence of the superfluid density in a non-centrosymmetric superconductor, *Phys. Rev. B* **73**, 024504 (2006).
- [41] Y. Higashi, Y. Nagai, T. Yoshida, Y. Masaki, and Y. Yanase, Robust zero-energy bound states around a pair-density-wave vortex core in locally noncentrosymmetric superconductors, *Phys. Rev. B* **93**, 104529 (2016).
- [42] Y. Yanase and M. Sigrist, Non-centrosymmetric superconductivity and antiferromagnetic order: Microscopic discussion of CePt₃Si, *J. Phys. Soc. Jpn.* **76**, 043712 (2007).
- [43] J. Goryo, M. H. Fischer, and M. Sigrist, Possible pairing symmetries in SrPtAs with a local lack of inversion center, *Phys. Rev. B* **86**, 100507(R) (2012).
- [44] S. J. Youn, M. H. Fischer, S. H. Rhim, M. Sigrist, and D. F. Agterberg, Role of strong spin-orbit coupling in the superconductivity of the hexagonal pnictide SrPtAs, *Phys. Rev. B* **85**, 220505(R) (2012).
- [45] K. Michaeli, A. C. Potter, and P. A. Lee, Superconducting and Ferromagnetic Phases in SrTiO₃/LaAlO₃ Oxide Interface Structures: Possibility of Finite Momentum Pairing, *Phys. Rev. Lett.* **108**, 117003 (2012).
- [46] Y. Nakamura and Y. Yanase, Multi-orbital superconductivity in SrTiO₃/LaAlO₃ interface and SrTiO₃ surface, *J. Phys. Soc. Jpn.* **82**, 083705 (2013).
- [47] Y. Nakamura and Y. Yanase, Odd-parity superconductivity in bilayer transition metal dichalcogenides, *Phys. Rev. B* **96**, 054501 (2017).
- [48] R. A. Klemm, A. Luther, and M. R. Beasley, Theory of the upper critical field in layered superconductors, *Phys. Rev. B* **12**, 877 (1975).
- [49] P. Giannozzi, S. Baroni, N. Bonini, M. Calandra, R. Car, C. Cavazzoni, D. Ceresoli, G. L. Chiarotti, M. Cococcioni, I. Dabo, A. D. Corso, S. de Gironcoli, S. Fabris, G. Fratesi, R. Gebauer, U. Gerstmann, C. Gougoussis, A. Kokalj, M. Lazzeri, L. Martin-Samos *et al.*, QUANTUM ESPRESSO: A modular and open-source software project for quantum simulations of materials, *J. Phys.: Condens. Matter* **21**, 395502 (2009).
- [50] T. Shirasawa, S. Yoshizawa, T. Takahashi, and T. Uchihashi, Structure determination of the Si(111)- $\sqrt{7} \times \sqrt{3}$ -In atomic-layer superconductor, *Phys. Rev. B* **99**, 100502(R) (2019).
- [51] U. Klein, D. Rainer, and H. Shimahara, Interplay of Fulde-Ferrell-Larkin-Ovchinnikov and vortex states in

- two-dimensional superconductors, *J. Low Temp. Phys.* **118**, 91 (2000).
- [52] M. Ichioka, H. Adachi, T. Mizushima, and K. Machida, Vortex state in a Fulde-Ferrell-Larkin-Ovchinnikov superconductor based on quasiclassical theory, *Phys. Rev. B* **76**, 014503 (2007).
- [53] Y. Higashi, Y. Nagai, T. Yoshida, and Y. Yanase, Vortex core structure in multilayered Rashba superconductors, *J. Phys.: Conf. Ser.* **568**, 022018 (2014).
- [54] Y. Dan and R. Ikeda, Quasiclassical analysis of vortex lattice states in Rashba noncentrosymmetric superconductors, *Phys. Rev. B* **92**, 144504 (2015).
- [55] P. W. Anderson, Theory of dirty superconductors, *J. Phys. Chem. Solids* **11**, 26 (1959).
- [56] The slight discrepancy between $T_c(0)$ and T_{c0} stems from the difference in their definition. T_{c0} is the T_c for an s -wave pair in the clean limit in the absence of the ASOC and magnetic field. T_{c0} is the temperature satisfying $1/\lambda = \sum_{n=0}^{n_c(T_{c0})} 1/(n+1/2)$, from which we estimate $\lambda \approx 0.298$. On one hand, $T_c(0)$ denotes the T_c at $H = 0$. In the simplest case (s -wave pair, isotropic Fermi surface, and $\delta = 0$), $T_c(0)$ is determined by solving $\psi_s = \lambda\pi T \sum_{|\omega_n| < \omega_c} \psi_s / \sqrt{\omega_n^2 + \psi_s^2}$. We estimate $\lambda \approx 0.323$ via $1/\lambda = \sum_{n=0}^{n_c(T)} 1/(n+1/2) + \ln(T/T_{c0})$ for the self-consistent solution of $T_c(0)/T_{c0} = 1.031$. For both estimates, we use the cutoff frequency $\omega_c = 7\pi T_{c0}$. The fact that $T_c(0)/T_{c0} > 1$ reflects the value of the coupling constant used to determine $T_c(0)$.
- [57] A. Finkel'stein, Suppression of superconductivity in homogeneously disordered systems, *Phys. B (Amsterdam)* **197**, 636 (1994).
- [58] M. Smidman, M. Salamon, H. Yuan, and D. Agterberg, Superconductivity and spin-orbit coupling in non-centrosymmetric materials: A review, *Rep. Prog. Phys.* **80**, 036501 (2017).
- [59] S. Yoshizawa, H. Kim, T. Kawakami, Y. Nagai, T. Nakayama, X. Hu, Y. Hasegawa, and T. Uchihashi, Impact of Surface Conditions on the Superconductivity of Si(111)-($\sqrt{7} \times \sqrt{3}$)-In, *e-J. Surf. Sci. Nanotechnol.* **13**, 151 (2015).
- [60] S. Yoshizawa, H. Kim, T. Kawakami, Y. Nagai, T. Nakayama, X. Hu, Y. Hasegawa, and T. Uchihashi, Imaging Josephson Vortices on the Surface Superconductor Si(111)-($\sqrt{7} \times \sqrt{3}$)-In using a Scanning Tunneling Microscope, *Phys. Rev. Lett.* **113**, 247004 (2014).
- [61] H. Nam, H. Chen, T. Liu, J. Kim, C. Zhang, J. Yong, T. R. Lemberger, P. A. Kratz, J. R. Kirtley, K. Moler, P. W. Adams, A. H. MacDonald, and C.-K. Shih, Ultrathin two-dimensional superconductivity with strong spin-orbit coupling, *Proc. Natl. Acad. Sci. USA* **113**, 10513 (2016).
- [62] Y. Higashi, Y. Nagai, and N. Hayashi, Impurity effect on the local density of states around a vortex in noncentrosymmetric superconductors, *JPS Conf. Proc.* **3**, 015003 (2014).
- [63] N. Hayashi, Y. Higashi, N. Nakai, and H. Suematsu, Effect of Born and unitary impurity scattering on the Kramer-Pesch shrinkage of a vortex core in an s -wave superconductor, *Phys. C (Amsterdam)* **484**, 69 (2013).
- [64] N. Hayashi, Y. Kato, P. A. Frigeri, K. Wakabayashi, and M. Sigrist, Basic properties of a vortex in a noncentrosymmetric superconductor, *Phys. C (Amsterdam)* **437-438**, 96 (2006).
- [65] N. Hayashi (private communications). The condition that the Green's functions are invariant under the transformation $\vec{k} \rightarrow -\vec{k}$ is satisfied at least in spatially uniform systems, when the SC order parameters on the split two FSs, $\Delta_{I,II}$, are invariant under $\vec{k} \rightarrow -\vec{k}$. However, strictly speaking, the condition is not satisfied in systems in the presence of the superflow (for instance, around a vortex core) or in the helical phase (a helical modulation wave vector violates the isotropy of the system) [33,38]; that is, the Green's functions are not invariant under $\vec{k} \rightarrow -\vec{k}$ in such systems.